

MARS CLIMATE DATABASE v6.1 DETAILED DESIGN DOCUMENT

(ESA Contract No.4000128572/19/NL/AS)

CNES Contract "Base de données climatique martienne"

F. Forget, E. Millour, T. Pierron, M. Vals and V. Zakharov (LMD)
and the MCD team

October 2022

Abstract

This is the Detailed Design Document for version 6.1 of the Mars Climate Database (MCD). It contains a detailed description of the database and addresses technical aspects of how the data is represented, manipulated and post-processed by the MCD access software. Instructions on how to install the MCD and use the provided access software and post-processing tools are given in the MCD v6.1 **User Manual**.

Contents

| | | |
|----------|---|-----------|
| 1 | Introduction | 4 |
| 2 | General Description of Database Contents | 5 |
| 2.1 | MCD Files | 5 |
| 2.2 | MCD Software | 5 |
| 2.3 | MCD Datasets and Datafiles | 5 |
| 2.4 | Database Grid Structure | 8 |
| 2.4.1 | Horizontal Structure | 8 |
| 2.4.2 | Vertical Structure | 8 |
| 2.4.3 | Temporal Structure | 11 |
| 3 | Dust Distribution and EUV Scenarios in the MCD | 11 |
| 3.1 | The EUV Scenarios | 11 |
| 3.2 | The Dust Scenarios | 12 |
| 3.2.1 | Parametrization of dust vertical distribution and particle size variations | 12 |
| 3.2.2 | Dust column optical depth variations | 13 |
| 3.2.3 | Prescribed high temporal resolution dust column optical depth variations | 17 |
| 3.2.4 | High temporal resolution dust deposition rate | 17 |
| 4 | Technical description of Methods Used to Retrieve Data from the MCD | 18 |
| 4.1 | Temporal Interpolations | 18 |
| 4.2 | Spatial Interpolations | 18 |
| 4.2.1 | Horizontal Interpolation | 18 |
| 4.2.2 | Vertical Interpolation | 18 |
| 4.2.3 | Specific Treatments of Vertical Interpolation | 19 |
| 5 | Variability Models in the MCD | 20 |
| 5.1 | Day-to-Day RMS of Variables | 20 |
| 5.2 | The Large-Scale Variability Model | 20 |
| 5.2.1 | Calculation of EOFs and PCs | 21 |
| 5.2.2 | Storage of variability with EOFs | 21 |
| 5.2.3 | Reconstructing a realistic variability | 22 |
| 5.2.4 | Reconstructing the inter-annual variability of the Martian atmosphere | 25 |
| 5.3 | The Small-Scale Variability Model | 25 |
| 6 | Post processing of short wave fluxes | 28 |
| 7 | High Resolution Outputs | 29 |
| 7.1 | High Resolution Topography and Areoid | 29 |
| 7.1.1 | Mars Gravity Model | 29 |
| 7.1.2 | MOLA Topography | 29 |
| 7.2 | Deriving High Resolution Surface Pressure | 30 |
| 7.3 | Computing High Resolution Values of Atmospheric Variables | 31 |
| 7.3.1 | Interpolation of Atmospheric Temperature | 31 |
| 7.3.2 | Interpolation of Density | 33 |
| 7.3.3 | Modification of Other Variables | 33 |
| 7.4 | Computation of the solar irradiance on the surface | 33 |
| 7.4.1 | Computation of the slope inclination and orientation | 33 |
| 7.4.2 | Computation of the solar irradiance on the slope | 37 |
| 7.5 | Computation of high resolution slope winds | 38 |
| 7.5.1 | The model | 38 |
| 7.5.2 | Calculation of the slope inclination and orientation to compute slope winds | 40 |
| 7.5.3 | Buoyancy term | 41 |
| 7.5.4 | Friction term | 41 |
| 7.5.5 | Stationary solution of the equations | 42 |

| | | |
|----------|---|-----------|
| A | Computing Martian Dates and Local Time | 43 |
| A.1 | Some constants | 43 |
| A.2 | Computing martian dates and aerocentric solar longitude | 43 |
| A.2.1 | The three anomalies | 43 |
| A.2.2 | Aerocentric solar longitude L_s | 43 |
| A.2.3 | Converting Julian date JD to Martian sol number D_s | 43 |
| A.2.4 | Converting sol number D_s date to L_s | 44 |
| A.3 | Computing Local True Solar Time | 44 |
| B | Differences Between Version 6.1 and Previous Versions of the MCD | 46 |

1 Introduction

The Mars Climate Database (MCD) is a database of atmospheric statistics compiled from state-of-the art Global Climate Model (GCM) simulations of the Martian atmosphere.

The LMD (Laboratoire de Météorologie Dynamique) Mars GCM, recently renamed the Mars Planetary Climate Model (PCM), computes in 3D the atmospheric circulation taking into account radiative transfer through the gaseous atmospheres as well as through dust and ice aerosols, includes a representation of the CO₂ ice condensation and sublimation on the ground and in the atmosphere, simulates the water cycle (with modelling of cloud microphysics), the dust multisize particle transport, the atmospheric composition controlled by the photochemistry and the local non-condensable gas enrichment and depletion induced by CO₂ condensation and sublimation. It has been extended into the thermosphere and model the ionospheric processes¹.

The model used to compile the statistics has been extensively validated using available observational data and aims at representing the current best knowledge of the state of the Martian atmosphere given the observations and the physical laws which govern the atmospheric circulation and surface conditions on the planet.

The Mars Climate Database access software adds several capabilities to better represent the Martian environment variability and accurately compute the surface pressure at high spatial resolution.

This document provides the user of the MCD with a detailed description of the database structure and of technical aspects of the access software.

¹. A detailed description of the Mars PCM is out of the scope of the present document. Nevertheless, details can be found in the scientific papers provided with the database in the `docs/articles` directory:

- `model_jgr99.pdf` : Reference description of the General Circulation Model used to make the Mars Climate Database (MCD) v1 (somewhat obsolete, but useful)
- `mcd_v1.0_jgr99.pdf` : Description of the MCDv 1.0 (somewhat obsolete, but useful).
- `dust_distribution_jgr2011.pdf` : Description of how the dust distribution was prescribed in the MCD v5 and validation with MGS TES observations (somewhat obsolete, but useful).
- `rocket_dust_storm_jgr2018.pdf` : Description of the rocket dust storm parametrization that is used in the simulations for a better representation of detached dust layers.
- `dust_climatology_icarus2015.pdf` : How the available dust opacity observations have been compiled to create the dust scenarios used to simulate Martian Years 24 to 34 in MCD v6.
- `water_clouds_jgr2004.pdf` : Includes a description of the water vapor, water cloud model used for MCD v4. (somewhat obsolete, but useful)
- `water_clouds_grl2013.pdf` : Describes the modeling of the radiatively active clouds (as done in MCD v5-6) and analyses their influence.
- `water_clouds_jgr2014.pdf` : Further description and details on the modeling of the water cycle with radiatively active clouds and an improved cloud microphysical model.
- `convection_pbl_jgr2013.pdf` : Describes the improved parametrisation of the turbulent/convection dynamics used since MCD v5.
- `ozone_jgr2004.pdf` : The chemistry-transport model used to predict ozone (since MCD v4)
- `ozone_nature2008.pdf` : More recent results from the chemistry-transport model used to predict ozone (MCD v5-6)
- `non_condensable_gas_2008.pdf` : An extended abstract describing the modeling of the non-condensable gas enrichment and depletion induced by the condensation and sublimation of CO₂ since MCD v5.
- `thermosphere_grl05.pdf` : Extension of the GCM to the thermosphere as done in MCD v4.
- `thermosphere_jgr2009.pdf` : A more detailed description of the extension of the GCM in the thermosphere as done since MCD v4.
- `thermosphere_variability_jgr2015.pdf` : Analysis and validation of the thermosphere variability simulated by the GCM from MY24 to MY31.
- `ionosphere_jgr2013.pdf` : A description of the photochemical ionosphere (from surface up to ~180km) in the model.

The MCD is freely available online at request. Its content may also be accessed to make plots and figures using the interactive server on our WWW site at:

<http://www-mars.lmd.jussieu.fr>

2 General Description of Database Contents

2.1 MCD Files

The MCD main directory contains three folders: `docs` which contains documentation, `data` which contains the datafiles and `mcd` which contains the access software (see the User Manual).

2.2 MCD Software

Subdirectory `mcd` contains the following Fortran programs:

- `MCD.F90`: This is the main module containing the main subroutine `call_mcd` which should be used to retrieve data from the database. The file also contains a collection of subsidiary routines. Input and output arguments of `call_mcd` are documented in the MCD User Guide.
- `test_mcd.F90`: A sample program provided to display (and test) the way to call subroutine `call_mcd` and to retrieve data from the MCD.

Apart from these Fortran programs, the `mcd` directory also contains a subdirectory `interfaces` containing subdirectories with examples of interfaces for other languages: `idl`, `matlab`, `python` and `c_interfaces` (which contains both C and C++ interface examples). See the accompanying README files and the MCD User Manual for details.

The subdirectory `testcase` contains a program allowing to check the MCD has been correctly installed.

2.3 MCD Datasets and Datafiles

MCD data is stored in various folders and files in directory `data` using the Network Common Data Form (NetCDF) developed and distributed by Unidata. The NetCDF libraries are freely available for numerous platforms from the Unidata web site:

<http://www.unidata.ucar.edu/software/netcdf>

- Essential and common datafiles
 - File `mountain.nc` which contains maps (at model resolution, i.e. a 64x49 longitude-latitude grid) of topography, areoid, sub-gridscale standard deviation of topography (useful for computing gravity wave perturbations), roughness length, surface thermal inertia, surface bare ground albedo and perennial surface water ice areas.
 - File `mola32.nc` which contains a high resolution (32 pixels per degree) map of Martian topography.
 - File `mgm1025` contains the spherical harmonic expansion coefficients necessary to compute the Martian areoid with high accuracy.
 - File `dust_high_resol` subdirectory containing the high temporal resolution dust opacity scenarios.
 - File `slope_map.nc` contains high resolution slope inclination and orientation for slope winds calculation.
- Individual dust scenarios (see section 3 for a detailed description) datafiles are in corresponding subdirectories:

- `clim_aveEUV`, `clim_minEUV` and `clim_maxEUV` for the baseline climatology² dust scenarios,
- `cold` for the cold scenario
- `warm` for the warm scenario
- `strm` for the dust storm scenario
- `MY24`, `MY25`, `MY26`, `MY27`, `MY28`, `MY29`, `MY30`, `MY31`, `MY32`, `MY33`, `MY34` and `MY35` for the Martian Year scenarios.

The file naming convention for each file is as follows :

Data Filename = ‘scen’_‘mon’_‘type’.nc for low atmospheric files (up to around 120km – 53 levels)

Data Filename = ‘scen’_‘mon’_‘thermo’_‘solar’_‘type’.nc for thermospheric files (from around 120km up to around 300km – 20 levels).

‘scen’ denotes the dust scenario type (`clim`, `cold`, `warm`, `strm`, `MY24`, `MY25`, etc.), where ‘mon’ denotes the month number:

‘mon’ = ‘01’ is month 1, $L_s = 0^\circ - 30^\circ$,

‘mon’ = ‘02’ is month 2, $L_s = 30^\circ - 60^\circ$,

‘mon’ = ‘03’ is month 3, $L_s = 60^\circ - 90^\circ$,

‘mon’ = ‘04’ is month 4, $L_s = 90^\circ - 120^\circ$,

‘mon’ = ‘05’ is month 5, $L_s = 120^\circ - 150^\circ$,

‘mon’ = ‘06’ is month 6, $L_s = 150^\circ - 180^\circ$,

‘mon’ = ‘07’ is month 7, $L_s = 180^\circ - 210^\circ$,

‘mon’ = ‘08’ is month 8, $L_s = 210^\circ - 240^\circ$,

‘mon’ = ‘09’ is month 9, $L_s = 240^\circ - 270^\circ$,

‘mon’ = ‘10’ is month 10, $L_s = 270^\circ - 300^\circ$,

‘mon’ = ‘11’ is month 11, $L_s = 300^\circ - 330^\circ$,

‘mon’ = ‘12’ is month 12, $L_s = 330^\circ - 360^\circ$,

‘mon’ = ‘all’ is the whole year for the Empirical Orthogonal Functions (EOF) data for the large-scale variability model.

‘type’ indicates the type of data in the file :

‘type’ = ‘me’ means “mean data”,

‘type’ = ‘sd’ means “standard deviation data” and “rms data”,

‘type’ = ‘eo’ means EOF data for large scale perturbations.

‘solar’ indicates the type of solar scenario for thermosphere files:

‘solar’ = ‘min’ for fixed minimum EUV,

‘solar’ = ‘ave’ for fixed average EUV,

‘solar’ = ‘max’ for fixed maximum EUV,

‘solar’ = ‘var’ for varying (ie. daily evolving) EUV.

Each of the `me` mean data files contain 12 mean values (for the given month) corresponding to 12 solar times of day (i.e. every 2 hours) for the variables shown in Table 1. The `sd` data files contain day-to-day RMS values of variables (see Table 2 for details).

Table 1: Variables stored in database mean data files

| Mean variable | symbol | units | 2-D or 3-D |
|---|--------------------------|--------------------|------------|
| Surface temperature | <code>tsurf</code> | K | 2-D |
| Surface pressure | <code>ps</code> | Pa | 2-D |
| CO ₂ ice cover | <code>co2ice</code> | kg m ⁻² | 2-D |
| LW (thermal IR) radiative flux to surface | <code>fluxsurf_lw</code> | W m ⁻² | 2-D |

²Note that only the `clim_aveEUV` directory is required; all others are optional, in the sense that they are only required when data for these specific scenarios is sought.

Table 1: Variables stored in database mean data files

| | | | |
|--|--------------------|---------------------------|-----|
| LW (thermal IR) radiative flux to space | fluxtop_lw | W m^{-2} | 2-D |
| SW (solar) incoming radiative flux to surface | fluxsurf_dn_sw | W m^{-2} | 2-D |
| SW (solar) direct incoming radiative flux to surface | fluxsurf_dir_dn_sw | W m^{-2} | 2-D |
| SW (solar) reflected radiative flux from surface | fluxsurf_up_sw | W m^{-2} | 2-D |
| SW (solar) outgoing radiative flux to space | fluxtop_up_sw | W m^{-2} | 2-D |
| SW (solar) incoming radiative flux from space | fluxtop_dn_sw | W m^{-2} | 2-D |
| Monthly mean visible Dust optical depth at 610 Pa | tau_pref_gcm | | 2-D |
| Water vapor column | col_h2ovapor | kg/m^2 | 2-D |
| Water ice column | col_h2oice | kg/m^2 | 2-D |
| Height of thermals in the PBL | zmax | m | 2-D |
| Maximum thermals heat flux | hfmax | K.m/s | 2-D |
| Vertical velocity scale in thermals | wstar | m/s | 2-D |
| H ₂ O ice cover (seasonal frost) | h2oice | kg m^{-2} | 2-D |
| CO ₂ column | c_co2 ³ | molecules/cm ² | 2-D |
| CO column | c_co ³ | molecules/cm ² | 2-D |
| O column | c_o ³ | molecules/cm ² | 2-D |
| O ₂ column | c_o2 ³ | molecules/cm ² | 2-D |
| O ₃ column | c_o3 ³ | molecules/cm ² | 2-D |
| H column | c_h ³ | molecules/cm ² | 2-D |
| H ₂ column | c_h2 ³ | molecules/cm ² | 2-D |
| N ₂ column | c_n2 ³ | molecules/cm ² | 2-D |
| Ar column | c_ar ³ | molecules/cm ² | 2-D |
| He column | c_he ³ | molecules/cm ² | 2-D |
| Total Electronic Content (TEC) | c_elec | electrons/cm ² | 2-D |
| Atmospheric density | rho | kg m^{-3} | 3-D |
| Atmospheric temperature | temp | K | 3-D |
| Zonal (East-West) wind | u | m s^{-1} | 3-D |
| Meridional (North-South) wind | v | m s^{-1} | 3-D |
| Vertical (up-down) wind | w | m s^{-1} | 3-D |
| Water vapor mixing ratio | vmr_h2ovapor | mol/mol | 3-D |
| Water ice mixing ratio | vmr_h2oice | mol/mol | 3-D |
| CO ₂ volume mixing ratio | vmr_co2 | mol/mol | 3-D |
| CO volume mixing ratio | vmr_co | mol/mol | 3-D |
| O volume mixing ratio | vmr_o | mol/mol | 3-D |
| O ₂ volume mixing ratio | vmr_o2 | mol/mol | 3-D |
| O ₃ volume mixing ratio | vmr_o3 | mol/mol | 3-D |
| H volume mixing ratio | vmr_h | mol/mol | 3-D |
| H ₂ volume mixing ratio | vmr_h2 | mol/mol | 3-D |
| N ₂ volume mixing ratio | vmr_n2 | mol/mol | 3-D |
| Ar volume mixing ratio | vmr_ar | mol/mol | 3-D |
| He volume mixing ratio | vmr_he | mol/mol | 3-D |
| Electron number density | vmr_elec | mol/mol | 3-D |
| Dust mass mixing ratio | dustq | kg/kg | 3-D |
| Dust effective radius | reffdust | m | 3-D |
| Water ice effective radius | reffice | m | 3-D |

The EOF datafiles (eo) contain normalized, multi-dimensional EOFs of zonal wind, meridional wind, atmospheric temperature and surface pressure as well as some normalization factors, eigenvalues and

³Note that the column is converted in kg m^{-2} when output from the MCD

| Day to day variabilities (RMS) Pressure-wise and/or altitude-wise | ARMS symbol | RMS symbol | units | 2-D or 3-D |
|--|----------------|-----------------|--------------------|---------------|
| Surface temperature | | rmstsurf | K | 2-D |
| Surface pressure | | rmsps | Pa | 2-D |
| Dust optical depth | | rmstau_pref_gcm | | 2-D |
| Atmospheric temperature | armstemp | rmstemp | K | 3-D |
| Atmospheric density | armsrho | rmsrho | kg m ⁻³ | 3-D |
| Zonal (East-West) wind | armsu | rmsu | m s ⁻¹ | 3-D |
| Meridional (North-South) wind | armsv | rmsv | m s ⁻¹ | 3-D |
| Vertical (down-up) wind | armw | rmsw | m s ⁻¹ | 3-D |
| Atmospheric pressure | armspressure | | Pa | 3-D |

Table 2: Variables stored in database standard deviation data files - lower atmosphere. For 3-D variables, the 'arms' prefix indicates an altitude-wise RMS and the 'rms' prefix a pressure-wise RMS.

| Day to day variabilities (RMS) Pressure-wise and/or altitude-wise | ARMS symbol | RMS symbol | units | 2-D or 3-D |
|--|----------------|---------------|--------------------|---------------|
| Atmospheric temperature | armstemp | rmstemp | K | 3-D |
| Atmospheric density | armsrho | rmsrho | kg m ⁻³ | 3-D |
| Zonal (East-West) wind | armsu | rmsu | m s ⁻¹ | 3-D |
| Meridional (North-South) wind | armsv | rmsv | m s ⁻¹ | 3-D |
| Vertical (down-up) wind | armsw | rmsw | m s ⁻¹ | 3-D |
| Atmospheric pressure | armspressure | | Pa | 3-D |

Table 3: Variables stored in database standard deviation data files - thermosphere. For 3-D variables, the 'arms' prefix indicates an altitude-wise RMS and the 'rms' prefix a pressure-wise RMS.

principal component model coefficients. It is recommended that you use the software supplied to access and exploit the data in these files.

2.4 Database Grid Structure

2.4.1 Horizontal Structure

Variables in the database are stored on the grid on which they are obtained from the general circulation model (GCM) runs: a regular, equispaced horizontal 64×49 grid⁴ in East longitude \times latitude. Longitudes thus range from -180.0° to 174.375° in steps of 5.625° and latitudes from 90° to -90° in steps of 3.75° .

2.4.2 Vertical Structure

Variables in the database are stored on the same vertical grid on which they are computed. This vertical coordinate is a hybrid coordinate in which vertical levels l are at pressure P :

$$P(l) = aps(l) + bps(l) \times P_S \quad (1)$$

where P_S is surface pressure. Coefficients $aps(l)$ and $bps(l)$ are respectively hybrid pressure and hybrid sigma levels.

In its present form the database extends over 73 levels and variables in the datafiles are split between lower atmosphere ($l = 1, \dots, 53$) and thermospheric ($l = 54, \dots, 73$, for thermo datafiles). This is due to the

⁴Technically, this grid is not exactly the computational grid: dynamical variables are in fact computed on a complementary staggered grid.

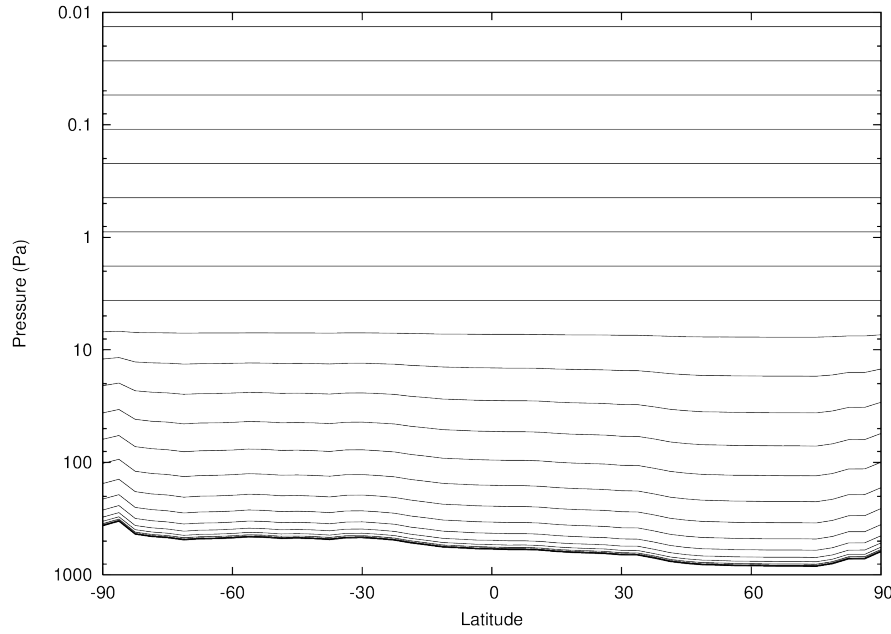


Figure 1: Illustration of the vertical hybrid coordinate system used to define MCD vertical levels. It follows the topography at low altitude and becomes equal to pressure in the free atmosphere. Note that not all levels are shown. The MCD vertical levels extend to much lower pressures, down to $P = 2.10^{-8}$ Pa for the last (73rd) level.

fact that only the thermosphere is affected by solar EUV input, unlike the lower part of the atmosphere. In order to reconstruct a column of data, one must thus extract the first 53 levels from 'lower atmosphere' datafiles and obtain the following 20 from the corresponding 'thermosphere' datafiles.

Note that *aps* and *bps* are prescribed coefficients such that near the surface (small values of *l*) levels are essentially terrain-following sigma coordinates, whereas at high altitude (large values of *l*) the vertical levels are pressure levels, as shown in Figure 1. Values of coefficients *aps* and *bps* are given in the following table, along with corresponding pseudo-altitude which are the approximative heights above local surface of the corresponding layer (computed using a surface pressure of 610 Pa and a scale height of 10 km; it is thus a rough estimate and particularly inaccurate in the upper atmosphere above 80 km because it does not account for actual changes in temperatures and scale height there).

| Layer | hybrid pressure level aps (Pa) | hybrid sigma level bps | Typical pressure (Pa) | pseudo-altitude above surface (km) |
|-------|--------------------------------|------------------------|-----------------------|------------------------------------|
| 1 | 0.004555349 | 0.9995446 | 609.7 | 0.0045 |
| 2 | 0.0239249 | 0.9976095 | 608.5 | 0.0235 |
| 3 | 0.07591269 | 0.9924263 | 605.4 | 0.0748 |
| 4 | 0.1893394 | 0.981167 | 598.7 | 0.187 |
| 5 | 0.400664 | 0.9603534 | 586.2 | 0.397 |
| 6 | 0.7374411 | 0.927568 | 566.6 | 0.739 |
| 7 | 1.182712 | 0.8848308 | 540.9 | 1.20 |
| 8 | 1.680694 | 0.8377352 | 512.7 | 1.74 |
| 9 | 2.190726 | 0.7901452 | 484.2 | 2.31 |
| 10 | 2.701583 | 0.742998 | 455.9 | 2.91 |
| 11 | 3.210279 | 0.6964362 | 428.0 | 3.54 |
| 12 | 3.71392 | 0.650592 | 400.6 | 4.21 |
| 13 | 4.209542 | 0.605603 | 373.6 | 4.90 |
| 14 | 4.694163 | 0.561609 | 347.3 | 5.63 |
| 15 | 5.164892 | 0.518743 | 321.6 | 6.40 |

..... table continued next page

| Layer | hybrid pressure level aps (Pa) | hybrid sigma level bps | Typical pressure (Pa) | pseudo-altitude above surface (km) |
|---------------------------------------|-----------------------------------|------------------------|-----------------------|---------------------------------------|
| 16 | 5.618903 | 0.4771346 | 296.7 | 7.21 |
| 17 | 6.053442 | 0.4369111 | 272.6 | 8.06 |
| 18 | 6.465924 | 0.3981894 | 249.4 | 8.95 |
| 19 | 6.853908 | 0.3610796 | 227.1 | 9.88 |
| 20 | 7.215168 | 0.3256798 | 205.9 | 10.9 |
| 21 | 7.547711 | 0.2920752 | 185.7 | 11.9 |
| 22 | 7.849764 | 0.2603408 | 166.7 | 13.0 |
| 23 | 8.119835 | 0.2305355 | 148.7 | 14.1 |
| 24 | 8.35673 | 0.2027013 | 132.0 | 15.3 |
| 25 | 8.559542 | 0.1768644 | 116.4 | 16.6 |
| 26 | 8.72765 | 0.1530335 | 102.1 | 17.9 |
| 27 | 8.860713 | 0.1312006 | 88.89 | 19.3 |
| 28 | 8.958645 | 0.1113394 | 76.88 | 20.7 |
| 29 | 9.02156 | 0.09340788 | 66.00 | 22.2 |
| 30 | 9.049708 | 0.07734737 | 56.23 | 23.8 |
| 31 | 9.043372 | 0.06308509 | 47.5 | 25.5 |
| 32 | 9.002701 | 0.0505361 | 39.83 | 27.3 |
| 33 | 8.927474 | 0.03960426 | 33.09 | 29.1 |
| 34 | 8.816672 | 0.03018546 | 27.23 | 31.1 |
| 35 | 8.667742 | 0.02217142 | 22.19 | 33.1 |
| 36 | 8.475095 | 0.01545468 | 17.90 | 35.3 |
| 37 | 8.226561 | 0.009935751 | 14.29 | 37.5 |
| 38 | 7.893226 | 0.005542601 | 11.27 | 39.9 |
| 39 | 7.390395 | 0.002297167 | 8.792 | 42.4 |
| 40 | 6.467072 | 0.0004982225 | 6.771 | 45.0 |
| 41 | 5.13999 | 1.159327e-05 | 5.147 | 47.8 |
| 42 | 3.856093 | 1.849162e-09 | 3.856 | 50.6 |
| 43 | 2.832351 | 1.103708e-16 | 2.832 | 53.7 |
| 44 | 2.020732 | 0. | 2.021 | 57.1 |
| 45 | 1.388545 | 0. | 1.389 | 60.9 |
| 46 | 0.9128612 | 0. | 0.9129 | 65.0 |
| 47 | 0.569452 | 0. | 0.5695 | 69.8 |
| 48 | 0.3336073 | 0. | 0.3336 | 75.1 |
| 49 | 0.1818931 | 0. | 0.1819 | 81.2 |
| 50 | 0.09301232 | 0. | 9.301e-02 | 87.9 |
| 51 | 0.04618855 | 0. | 4.619e-02 | 94.9 |
| 52 | 0.02293656 | 0. | 2.294e-02 | 102 |
| 53 | 0.01138996 | 0. | 1.139e-02 | 109 |
| 54 | 0.005656085 | 0. | 5.656e-03 | 116 |
| 55 | 0.002808729 | 0. | 2.809e-03 | 123 |
| 56 | 0.001394773 | 0. | 1.395e-03 | 130 |
| 57 | 0.000692624 | 0. | 6.926e-04 | 137 |
| 58 | 0.0003439469 | 0. | 3.439e-04 | 144 |
| 59 | 0.000170799 | 0. | 1.708e-04 | 151 |
| 60 | 8.481626e-05 | 0. | 8.482e-05 | 158 |
| 61 | 4.211851e-05 | 0. | 4.211e-05 | 165 |
| 62 | 2.091543e-05 | 0. | 2.092e-05 | 172 |
| 63 | 1.03863e-05 | 0. | 1.039e-05 | 179 |
| 64 | 5.157682e-06 | 0. | 5.158e-06 | 186 |
| 65 | 2.561229e-06 | 0. | 2.561e-06 | 193 |
| 66 | 1.271869e-06 | 0. | 1.272e-06 | 200 |
| 67 | 6.315913e-07 | 0. | 6.316e-07 | 207 |
| 68 | 3.13639e-07 | 0. | 3.136e-07 | 214 |
| 69 | 1.557485e-07 | 0. | 1.557e-07 | 221 |
| 70 | 7.734241e-08 | 0. | 7.734e-08 | 228 |
| table continued next page | | | | |

| Layer | hybrid pressure level aps (Pa) | hybrid sigma level bps | Typical pressure (Pa) | pseudo-altitude above surface (km) |
|-------|-----------------------------------|------------------------|-----------------------|---------------------------------------|
| 71 | 3.840711e-08 | 0. | 3.841e-08 | 235 |
| 72 | 1.907241e-08 | 0. | 1.907e-08 | 242 |
| 73 | 9.471076e-09 | 0. | 9.471e-09 | 249 |

2.4.3 Temporal Structure

In order to store the seasonal behaviour of variables, data from the Global Climate Model was processed to be stored along 12 martian months. Each of these month is defined as spanning 30° in solar longitude (months are thus “centered” on solar longitudes $L_s = 15^\circ, 45^\circ, \dots$). Due to the eccentricity of Mars’ orbit, martian months vary from 46 to 66 sols (martian solar days) long, as shown in Table 5.

Time evolution of variables on the scale of a sol is included in the datafiles where values at 12 times of day are stored. Martian hours are defined as being $1/24$ th of a sol. To avoid confusion, we do not use (or define) martian minutes or seconds: any martian time of day is always given as a fraction of a sol or in martian hours and decimal fractions thereof (e.g. $time = 18.5$ hours means 18 hours and a half).

The database reference time is Mars Universal Time (which is simply “prime meridian time”, i.e. the local time at 0° longitude) and data is stored every 2 martian hours, i.e. from 2 to 24 hours. Note that all times are expressed in True Solar Time (the sun is highest at noon) and not Mean Solar Time (see the description of the Equation Of Time in Appendix A).

The Local True Solar Time $LTST$ at a given East longitude lon (expressed in degrees) may easily be computed from the Local True Solar Time at longitude zero $LTST_0$ (i.e. Mars Universal Time) by the following formula:

$$LTST = LTST_0 + lon/15 \quad (2)$$

3 Dust Distribution and EUV Scenarios in the MCD

Combinations of dust and solar scenarios are provided because these are the two forcings that are highly variable from year to year.

- On the one hand, the solar conditions describe variations in the Extreme UV input which control the heating of the atmosphere above 120 km, which typically varies on a 11 years cycle. Depending on the scenarios, either fixed solar maximum average and/or minimum conditions or realistic (evolving daily) solar conditions are used.
- On the other hand, the major factor which governs the variability in the Martian atmosphere is the amount and distribution of suspended dust. Because of this variability, and since even for a given year the details of the dust distribution and optical properties can be uncertain, multi-annual model integrations were carried out for the database assuming various “dust scenarios”, i.e. prescribing various amount of airborne dust in the simulated atmosphere.

How these dust and EUV scenarios are taken into account is detailed in the following subsections.

3.1 The EUV Scenarios

The radiative output of the Sun is known to vary at different timescales: for example, due to the solar flares (timescale of minutes to hours), to the solar rotation (27 days) or to the magnetic cycle of the Sun (11 years, the so-called solar cycle). This last variability, first detected counting the number of sunspots, is more important in the UV (than in the visible) region of the solar spectrum, as a variability of about a factor 2 in the total EUV irradiance (below 120 nm) with the solar cycle is found. Although the UV spectral region represents a small contribution to the total solar energy, the UV radiation is the major

| Month number | Solar longitude range | Duration (in sols) |
|--------------|-----------------------|--------------------|
| 1 | 0 - 30 | 61 |
| 2 | 30 - 60 | 66 |
| 3 | 60 - 90 | 66 |
| 4 | 90 - 120 | 65 |
| 5 | 120 - 150 | 60 |
| 6 | 150 - 180 | 54 |
| 7 | 180 - 210 | 50 |
| 8 | 210 - 240 | 46 |
| 9 | 240 - 270 | 47 |
| 10 | 270 - 300 | 47 |
| 11 | 300 - 330 | 51 |
| 12 | 330 - 360 | 56 |

Table 5: Length of martian months. Note that a martian year is 668.6 sols (martian solar days) long and that a sol is 88775.245 seconds long; For convenience, the durations given above are rounded to be integer values.

heating source of the Martian upper atmosphere (above about 120 km). So, its variability has a strong impact over the thermospheric temperatures.

The EUV flux is represented in two manners in the MCD.

- In some of the MCD simulations, the EUV flux is set to constant values chosen to provide an estimation of the average and extreme (minimum and maximum) fluxes. The “**Solar maximum**” scenario corresponds to conditions when the solar cycle is at its maximum activity (value for E10.7⁵ at Earth around 320) and the UV emission is highest. For such conditions, a rise in temperatures in the thermosphere, induced by a more intense UV heating, is expected (and obtained). On the opposite, the “**Solar minimum**” scenario is appropriate for conditions when the sun is at its minimum activity (approximate value of E10.7 at Earth around 80). In this case, UV emission is low, so a lower temperature due to a lower UV heating is expected. The “**Solar average**” scenario is an intermediate situation between maximum and minimum solar activity (approximate value for E10.7 at Earth 140) Figure 2 displays mean temperature profiles corresponding to the three EUV scenarios.
- Simulations were also performed with a realistically (daily) evolving EUV input, taken from available E10.7 measurements, over the Martian years 24-35. Figure 2 also displays the mean thermospheric profiles corresponding to some of these martian years.

3.2 The Dust Scenarios

This section outlines the dust distribution scenarios used for the GCM integrations which make up the Mars Climate Database.

3.2.1 Parametrization of dust vertical distribution and particle size variations

In our simulations, at every location and time, the total dust column optical depth is prescribed to match the available observations. However, the dust vertical distribution and the dust particle size is computed online by the global climate model. This is detailed in the joined scientific paper (file `dust_distribution-jgr2011.pdf`) by Madeleine et al. (2011). In summary:

⁵E10.7 is a proxy for the integrated extreme ultraviolet flux from 1 to 105 nm expressed in the same unit than the canonic F10.7 index (full-disc solar emission at the 10.7 nm wavelength, expressed in units of $10^{-22} \text{ W m}^{-2} \text{ Hz}^{-1}$) originally measured by Earth-based radio-observatory when no solar spectral EUV fluxes is available.

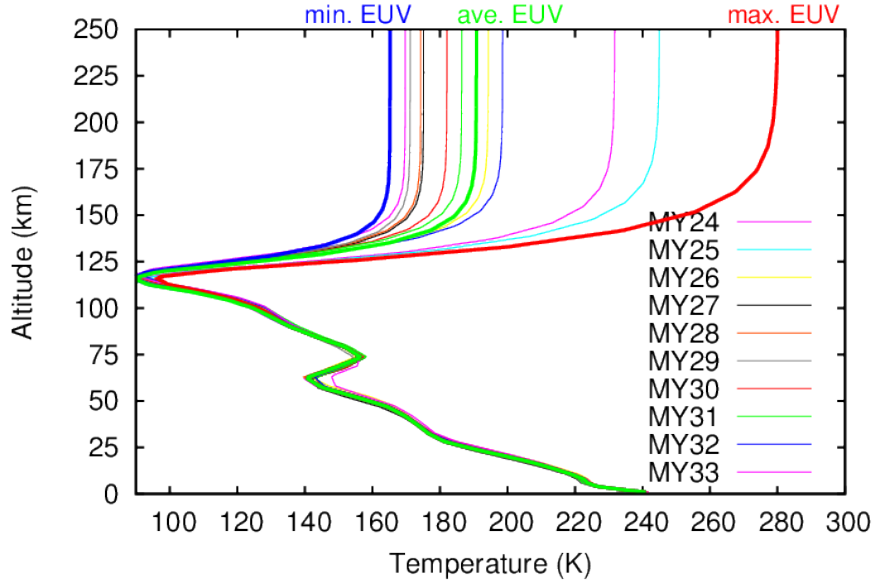


Figure 2: Illustration of temperature profiles at a given location provided by the GCM (with the same “clim” dust scenario) with the Extreme Ultraviolet (EUV) fluxes corresponding to the daily evolution observed during Martian Years 24-33 as well as the solar EUV minimum (min), average (ave) and maximum (max) scenarios.

1. **Dust vertical distribution:** In the global climate model, the dust vertical distribution is now estimated by following idealized dust-like tracers. The dust distribution is controlled by the balance between general circulation and gravitational sedimentation.
2. **3D variation of dust particle radii.** By transporting two moments of the dust fields (mass mixing ratio and number mixing ratio), the above scheme is used to simulate the gravitational segregation of larger dust particles and realistically simulate the decrease of dust effective radius in the vertical.
3. **Dust Single Scattering Properties.** We now use improved indexes of refraction provided by M. Wolff based on a variety of orbital and in-situ observations, and compute the single scattering properties of various dust size distributions using T-matrix theories following Wolff et al. *J. Geophys. Res.*, 112, E08S16 (2009). We have found that these properties allow for the first time to reconcile the observed amount of dust in the atmosphere with the temperatures observed simultaneously.
4. **Impact of dust scavenging by water ice condensation.** The condensation of ice particles is now taken into account to physically increase the sedimentation rate of the dust particles on which water ice has condensed.

3.2.2 Dust column optical depth variations

1. The “**Climatology**” (clim) scenario is derived from the available observations of dust from multiple years between $L_s \sim 105^\circ$ in Martian year ⁶ 24, 26, 27, 29, 30, 31, 32, 33 (years without global planet-encircling dust storms).

For this purpose, we carefully gathered and combined all available observations for each available year to reconstruct the dust field and its evolution as described in the joined paper (file `dust_climatology_icar` by Montabone et al. (2015)). In summary we used observations of the Martian atmosphere from

⁶This widely used numbering of martian years follows the calendar proposed by R. Todd Clancy (Clancy et al., *Journal of Geophys. Res.* 105, p 9553, 2000) which begins on April 11, 1955 ($L_s=0^\circ$)

April 1999 to July 2013 by different orbiting instruments: the Thermal Emission Spectrometer (TES) on board Mars Global Surveyor, the Thermal Emission Imaging System (THEMIS) on board Mars Odyssey, and the Mars Climate Sounder (MCS) on board Mars Reconnaissance Orbiter (MRO). The data have been gridded and interpolated using a kriging method.

Figure 3 present the seasonal evolution of the zonal mean dust opacity for the first 8 available Martian years.

To make the “climatic” simulation and estimate the reference simulations, we performed several sets of simulations:

- Mean atmospheric fields and their day-to-day variability are retrieved from a simulation performed using an averaged “climatic” dust scenario obtained by using the geometric mean the dust column optical depth from Martian years 24, 26, 27, 29, 30, 31, 32, 33 (years without global dust storm).
- As detailed in Section 5.2.4, the Large-scale variability perturbations provided with the clim scenario include a realistic interannual variability obtained by retrieving statistics from 6 independent simulations performed using Martian years 24, 26, 27, 29, 30, 31, 32, 33 dust scenarios.

This “Climatology” scenario is provided with 3 solar EUV conditions: solar min, solar ave, solar max.

2. The **cold scenario** corresponds to an extremely clear atmosphere (“Low dust scenario”). At a given seasonal date (Ls) and location, the dust opacity is set to be the minimum observed over Mars years 24-34, further decreased by 50%, topped with a solar minimum thermosphere (figure4).
3. The **warm scenario** corresponds to “dusty atmosphere” conditions, but nonetheless non-global dust storm conditions. The dust opacity at a given location and seasonal date (Ls) is set to the maximum observed over all Mars years (MY24-MY34), except during the MY25, MY28 and MY34 global dust storms, further increased by 50%, topped with a solar maximum thermosphere (figure5).
4. The **dust storm scenario** represents Mars during extreme global dust storms. The dust opacity is set to $\tau = 5$ at all times and over the whole planet. Moreover the dust optical properties are for this case set to represent “darker dust” than nominal (in practice for these runs, dust properties from Ockert-Bell et al. (*J. Geophys. Res.*, 102, 9039-9050, 1997) were used, rather than the more recent properties from Wolff et al. *J. Geophys. Res.*, 112, E08S16, 2009) used for all other MCD simulations).

This scenario is only provided for when such storms are likely to happen, during northern fall and winter (Ls=180-360), but with 3 cases of solar EUV inputs: solar min, solar ave, solar max.

Because the most intense phases of global dust storms (i.e. with visible opacities larger than 3) only last for a few weeks, to ensure a realistic behaviour of the water and CO₂ cycle (and the associated pressure cycle), the dust sorm simulations are started from initial states retrieved from the reference “clim” scenario at the beggining of each Martian months. In other words, the MCD dust storm scenario provides statistics on a Martian atmosphere experiencing a typical intense Ls=30° long dust storm. This scenario remains extreme because the atmosphere react very quickly to the onset of such an intense dust storm. Nevertheless this allows to capture in the statistics the variability induced by the onset of the dust storms.

5. The **Mars years scenarios**, MY24, MY25, MY26, MY27, MY28, MY29, MY30, MY31, MY32, MY33 and MY34. As already mentionned, we have access to the daily evolution of Martian atmospheric dust loading as well as to the daily evolution of the EUV received at Mars from the Sun for Mars years 24 to 34. The associated outputs correspond to our best representation of the Martian climate over these specific years.

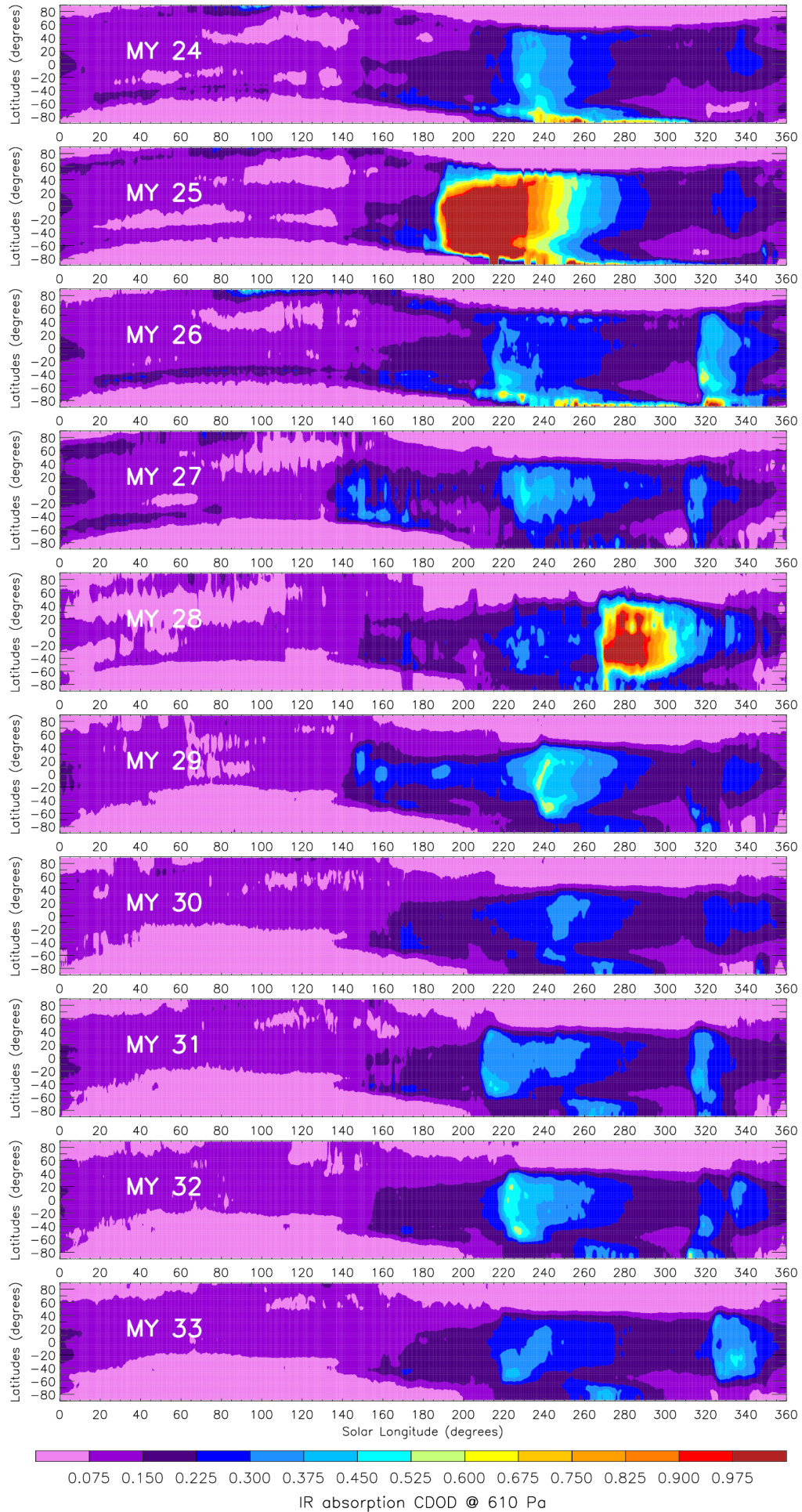


Figure 3: Dust scenarios derived from available observations and used as inputs to compute the database simulations. This figure shows the zonal means of dust absorption optical depth at infrared wavelength $9.3 \mu\text{m}$ (referred to pressure level 610 Pa) as a function of latitude and solar longitude for all available Martian years. These infrared dust column opacities are converted to extinction visible dust opacities by multiplying them by a factor of 2.6.

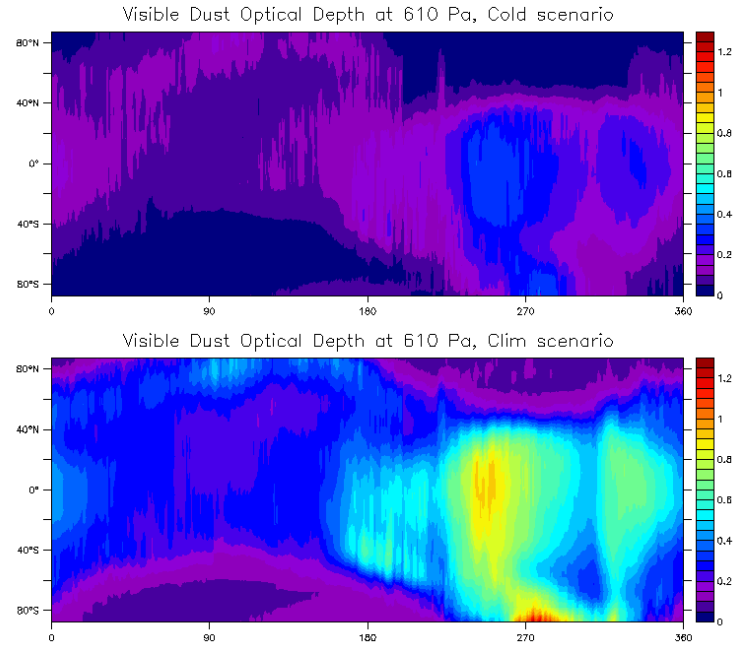


Figure 4: Seasonal evolution of the visible dust optical depth for the “cold” scenario (top plot), along with the reference “clim” scenario (bottom plot) for comparison (the same color scale is used for both plots).

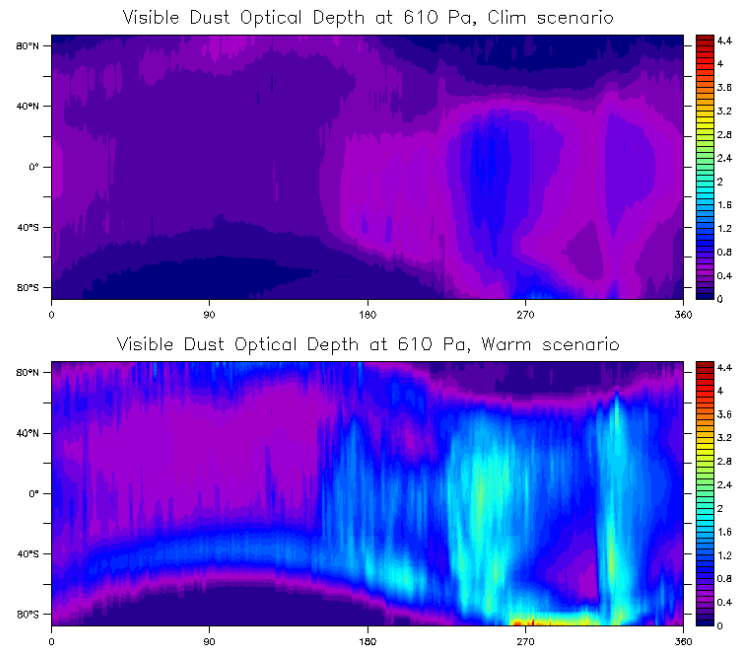


Figure 5: Seasonal evolution of the dust visible optical depth for the “warm” scenario (bottom plot), along with the “clim” scenario (top plot) for comparison (the same color scale is used for both plots).

3.2.3 Prescribed high temporal resolution dust column optical depth variations

The scenarios files, containing the dust optical depth at $9.3\mu\text{m}$ at 610 Pa, were used to run the GCM. As all data stored in the database, the optical depth, averaged on 30° of L_s is available as an output of the MCD. In addition of this averaged dust opacity, we added in the database the scenario files including one value of the dust opacity per day during one Martian year (considered as 669 sols) at every location of a 120×60 longitude-latitude grid. All the scenarios presented in the previous section are stored in the database in the directory 'dust_high_resol'.

One can extract the value of this high temporal resolution dust opacity using the 'call_mcd' subroutine. A bilinear interpolation in space and a linear interpolation in time is used to compute the value of opacity at the desired location and time prescribed by the user. The output is given as the dust optical depth in the visible above surface. In order to convert the dust opacity from dust opacity in the infrared (at $9.3\mu\text{m}$) at 610 Pa to extinction dust opacity in the visible, we use :

$$\tau_{ext}(9.3\mu\text{m}) = 1.3\tau_{abs}(9.3\mu\text{m}), \quad \tau_{ext}(vis) = 2\tau_{ext}(9.3\mu\text{m}) \quad (3)$$

$$\tau_{vis} = \frac{P_s}{610} \tau_{vis}(610\text{Pa}) \quad (4)$$

3.2.4 High temporal resolution dust deposition rate

The dust deposition rate R_{dust} (in $\text{kg.m}^{-2}.\text{s}^{-1}$) is computed as follows :

$$R_{\text{dust}} = mmr \times \rho \times W_s \quad (5)$$

with mmr the mass mixing ratio of the dust near the surface, ρ the dust density and W_s the Stokes speed at which the dust falls. The latter is computed with the formula from Rossow (1978) :

$$W_s = \frac{2}{9} \frac{\rho g}{\mu} r_{\text{sed}}^2 \left(1 + \beta \frac{4}{3} a \frac{T}{P_{\text{surf}} \times r_{\text{sed}}} \right) \quad (6)$$

with ρ the dust density, μ the air molecular viscosity, g the acceleration of gravity, β a coefficient to take into account non-sphericity of dust particle, $a(T/P_{\text{surf}})$ the gas mean free path, $r_{\text{sed}} = r_{\text{eff}}(1 + \nu_{\text{eff}})^2$ the average particle radius for sphericity (deduced from the dust distribution effective radius r_{eff} and the effective variance of the dust size distribution ν_{eff}). The values for dust properties ($r_{\text{eff}}, \nu_{\text{eff}}$) are given and discussed in Wolff *et al.* (2009). These parameters are set to the following values :

$$\left\{ \begin{array}{l} \rho = 2500 \text{ kg.m}^{-3} \\ \mu = 10^{-5} \text{ Pa.s} \\ g = 3.72 \text{ m.s}^{-2} \\ \beta = 0.5 \\ a = 1.6 \cdot 10^{-5} \text{ m.Pa.K}^{-1} \\ r_{\text{eff}} = 2.0 \cdot 10^{-6} \text{ m} \\ \nu_{\text{eff}} = 0.5 \end{array} \right.$$

The mass mixing ratio is a function of the dust opacity τ of the atmosphere. We use the high temporal resolution opacity, described in the previous section. It depends also on the single scattering extinction coefficient $Q_{\text{ext}} = 2.4$ and the surface pressure P_{surf} :

$$mmr = \frac{4}{3} \frac{\rho r_{\text{eff}} \tau}{Q_{\text{ext}} P_{\text{surf}}} \frac{g}{P_{\text{surf}}} \quad (7)$$

4 Technical description of Methods Used to Retrieve Data from the MCD

4.1 Temporal Interpolations

Once the time of year and of day at which data is requested is known (see Appendix A for details on how these can be computed for a given Julian date), linear interpolation between datasets of encompassing months along with linear interpolation between encompassing stored martian hours are used to evaluate data on the GCM grid.

4.2 Spatial Interpolations

4.2.1 Horizontal Interpolation

To compute the values of variables at a given location (which is not on the GCM grid), one needs to first build a virtual column of data along what would have been GCM levels. This profile is obtained by horizontal interpolation of encompassing grid values. To be specific, values of variables are obtained from encompassing grid values using bilinear interpolation, except for density ρ (and similar bi-products such as associated RMS or surface pressure), which is obtained using bilinear interpolation of $\log(\rho)$.

4.2.2 Vertical Interpolation

In order to compute the value of meteorological variables at a given height (or pressure), one must first identify the altitudes (and pressure) of the vertical levels of the profile. This is done by integrating the hydrostatic equation over the column:

$$\frac{\partial P}{\partial z} = -g \cdot \rho = -g \cdot \frac{P}{R \cdot T} \quad (8)$$

from which the relation between an increment in altitude δz and average (over δz), gas constant R_m , atmospheric temperature $T_m = \delta T / \log(\delta T)$, and log pressure increment $\delta \log P$ can be derived:

$$\delta z = -\frac{R_m}{g_m} \cdot T_m \cdot \delta \log P \quad (9)$$

This relation can be used to compute the altitudes of all the levels of a profile for which pressure $P(l)$ (or equivalently sigma levels $\sigma(l) = P(l)/P_S$, where P_S is surface pressure), atmospheric temperature $T(l)$ as well as gas constant $R(l)$ at all l levels are known. Moreover, as the database extends to high altitudes, it must also taken into account that gravity g varies as the inverse square of the distance to the center of the planet, i.e. that gravity at altitude z can be approximated as $g(z) = g_0 \cdot a_0^2 / (a_0 + z)^2$, where z is the altitude above the areoid a_0 , and $g_0 = 3.7257964 \text{ m/s}^2$ is the gravity at $a_0 = 3.39610^6 \text{ m}$.

The altitude of the first atmospheric layer is thus obtained using:

- Gravity $g(l = 1)$ is approximated to be that at the surface (of known orography, i.e. altitude above areoid, h):

$$g(l = 1) = g_0 \cdot a_0^2 / (a_0 + h)^2$$

- The altitude of the first layer is then simply

$$z(l = 1) = -[R(l = 1)/g(l = 1)] \cdot T(l = 1) \cdot \log(\sigma(l = 1))$$

From there, the altitudes of layers are recursively determined; i.e. for layer $l + 1$:

- Approximate $g(l + 1)$ using the altitude $z(l)$ of previous layer:

$$g(l + 1) = g_0 \cdot a_0^2 / (a_0 + h + z(l))^2$$

- Compute altitude of level $l + 1$:

$$z(l + 1) = z(l) - [R(l + 1)/g(l + 1)].T(l + 1). \log[\sigma(l + 1)/\sigma(l)]$$

Once the altitudes $z(l)$ of layers are known, then the value of a variable X at a given altitude above the surface z_s may be obtained from linear interpolation of values at encompassing grid points. For variables which are, to first order, exponentially distributed in altitude (e.g. pressure, density and associated variables) then the interpolation must naturally be performed on the logarithm of these values.

4.2.3 Specific Treatments of Vertical Interpolation

Interpolation, as explained above, is feasible when the altitude (or pressure) at which the value of a variable is sought falls in the range of the MCD grid. In the more extreme cases, either above the topmost atmospheric layer or below the lowest one, different approaches must be used. These are detailed here.

Above the MCD Topmost Layer

If above the MCD topmost layer $l = L$, then the concentration of component j of the neutral atmosphere at the altitude z_s is:

$$n_j(z_s) = n_j(L) \frac{T(L)}{T(z_s)} \exp\left\{-\int_{z(L)}^{z_s} \frac{g(z)}{R_j T(z)} dz\right\} \quad (10)$$

where n_j and R_j are the concentration and gas constant of specie j (in $\text{m}^2 \text{s}^{-2} \text{K}^{-1}$). This results from the fact that, in the upper thermosphere and exosphere the collision rate of molecules and atoms is so small that each species tend to have its own scale height.

Assuming that the gravity decreases inversely to the square of planetocentric radial coordinate as:

$$g(z) = g(L) \left(\frac{a_0 + h + z(L)}{a_0 + h + z} \right)^2 \quad (11)$$

Neglecting by the variation of neutral temperature with altitude $T(z > z(L)) \cong T(L)$ the pressure $P(z_s)$ at altitude z_s is:

$$P(z_s) = \sum_j P_j(L) \exp\left\{-\frac{g(L)}{R_j T(L)} \frac{(a_0 + h + z(L))(z_s - z(L))}{a_0 + h + z_s}\right\} \quad (12)$$

With $P_j(L)$ the partial pressure of specie j in the top layer of the model. When the vertical coordinate is requested in pressure units the conversion into meters is implemented numerically by the bisection method with 5% precision. Therefore, small discrepancies between cases with vertical coordinate defined in [Pa] and [m] may happen.

The pressure and volume mixing ratios of neutral species are computed according to these relations but all other variables (e.g. winds) are not extrapolated and are assumed to remain constant above the topmost layer.

The density and its variability are extrapolated above surface at altitude z_s as follows :

$$a(z_s) = a(L) \sum_j \frac{P(L)}{R_j T(L)} \frac{vmr_j(L)}{\rho(L)} \exp\left\{-\frac{g(L)}{R_j T(L)} \frac{(a_0 + h + z(L))(z_s - z(L))}{a_0 + h + z_s}\right\} \quad (13)$$

where a is either the density ρ or the density variability ρ_{rms} .

Below the Lowest MCD Layer

When below the lowest MCD layer $l = 1$ (which typically lies at 5 m above the surface, see table in Section 2.4.2), then pressure $P(z_s)$ at altitude z_s above the surface is computed using a hydrostatic vertical profile, i.e.:

$$P(z_s) = P(1) \exp [(z(1) - z_s).g(z_s)/(R(1).T(1))]$$

where $P(1)$, $R(1)$ and $T(1)$ are the pressure, gas constant and temperature at the first layer, $z(1)$ its altitude and $g(z_s)$ is gravity at altitude z_s . This formulation enables recovery of the value of surface pressure P_s when $z_s = 0$.

Density ρ , as well as the RMS of these two variables, are treated similarly.

Other variables (except horizontal winds and atmospheric temperature) are not extrapolated and are taken to be constant from the middle of the first atmospheric level down to the surface.

Near Surface Atmospheric Temperature and winds

Below the lowest MCD layer, temperature and winds are estimated using the Monin-Obukhov similarity theory which take into account the stability of the atmosphere (via its Richardson number), the sub-grid scale gustiness and the roughness length z_0 .

The values of the horizontal winds are set to zero below the roughness length z_0 .

5 Variability Models in the MCD

5.1 Day-to-Day RMS of Variables

The MCD provides the day-to-day variability of variables computed from the outputs of the Global Circulation Model (GCM). This day-to-day RMS of variable X is computed over each month as:

$$RMS(X) = \sqrt{\frac{1}{N} \sum_1^N \left(\langle X \rangle_{1 \text{ sol}} - \langle X \rangle_{10 \text{ sols}} \right)^2} \quad (14)$$

where N is the number of samples from the time-series output of variable X over the month and $\langle X \rangle_{1 \text{ sol}}$ and $\langle X \rangle_{10 \text{ sols}}$ respectively denote running averaged values of X over a sol and 10 sols.

The RMS thus obtained represents the variability of a variable from one day to the next, at a given time of the day, regardless of the general drift over the month (removed by taking into account the deviation of diurnal values to 10-day averages, i.e. long term trends, in the computation of the RMS).

It is important to note that the RMS values obtained from the GCM outputs are computed on the GCM grid and that since the vertical coordinate is essentially (see Section 2.4.2) a pressure coordinate, the obtained RMS values are evaluated at constant pressure.

Apart from this pressure-wise RMS, the MCD now also provides altitude-wise RMS, which is computed in the same way, but on time series of GCM outputs which have been interpolated on a fixed altitude vertical coordinate grid. For some variables, which are dependent on pressure, e.g. density, the difference between pressure-wise and altitude-wise RMS can be quite significant.

5.2 The Large-Scale Variability Model

In the MCD, data are stored in 12 monthly bins and at 12 local times of day. Although this captures the main seasonal and diurnal components of variability, any intra-month or day-to-day (synoptic) variations are averaged out. Thus there is a need to simulate this variability, especially if the user wishes to produce an ensemble of realizations of a variable at a particular seasonal date and local time of day which covers a realistic range of variability.

For this purpose, we store the 3D variability of pressure, temperature and winds using Empirical Orthogonal Functions (EOFs) over the different simulated years.

5.2.1 Calculation of EOFs and PCs

Consider a time series of longitude-pressure vectors of zonal wind, $u(\phi, p, t)$, meridional wind, $v(\phi, p, t)$, temperature, $T(\phi, p, t)$ and surface pressure $p^*(\phi, t)$ at M discrete time points and on L spatial points. We form a time series of vectors $\mathbf{D}(t)$, where

$$\mathbf{D}(t) = (\hat{u}(\phi, p, t), \hat{v}(\phi, p, t), \hat{T}(\phi, p, t), \hat{p}^*(\phi, t)) \quad (15)$$

and the hat $\hat{\cdot}$ denotes a removal of the series mean and normalization of variance operator,

$$\bar{u} = \frac{1}{ML} \sum_{m=1}^M \sum_{l=1}^L u_{ml} \quad (16)$$

$$\hat{u}_{ml} = \frac{u_{ml} - \bar{u}}{\sqrt{\frac{1}{ML} \sum_{m=1}^M \sum_{l=1}^L (u_{ml} - \bar{u})^2}} \quad (17)$$

where the m denotes time and the l denotes spatial point. Hence, with this normalization, the variance of the entire time series of $\mathbf{D}(t)$ is unity.

We then form the $(N \times N)$ covariance matrix, \mathbf{C} , such that

$$\mathbf{C} = \frac{1}{N} \mathbf{D} \mathbf{D}^T \quad (18)$$

where $N = (\text{number of horizontal points}) \times (3 \times \text{number of vertical points} + 1)$, \mathbf{D} is the $(N \times M)$ matrix whose rows are the vectors $\mathbf{D}(t)$ and the superscript T indicates the transpose.

The matrix \mathbf{C} is real symmetric and we can find the eigenvectors and eigenvalues and order them in decreasing eigenvalue magnitude. We note that if \mathbf{E}_i is the i th eigenvector then

$$|\mathbf{E}_i| = 1 \quad (19)$$

where $|\cdot|$ is the Euclidean Norm, and

$$\sum_{i=1}^N \lambda_i = 1 \quad (20)$$

where λ_i is the i th eigenvalue.

The i th principal component (PC) at time m , p_{mi} is defined as

$$p_{mi} = \sum_{n=1}^N D_{mn} E_{ni} = \mathbf{D} \cdot \mathbf{E}_i \quad (21)$$

and we note the result

$$\frac{1}{MN} \sum_{m=1}^M (p_{mi})^2 = \lambda_i \quad (22)$$

Each principal component has 669 values during one year (one per day).

5.2.2 Storage of variability with EOFs

As described above using PCs and their smoothed version provides a mean to store variability.

In practice, any state vector $V(\text{lon}, \text{lat}, \text{alt}, \text{time})$ can be decomposed as:

$$V(\text{lon}, \text{lat}, \text{alt}, \text{time}) = AVE(\text{lon}, \text{lat}, \text{alt}) + NORM(\text{lat}) \sum_i PC_i(\text{time}) \times EOF_i(\text{lat}, \text{lon}, \text{alt})$$

Where $AVE(\text{lon}, \text{lat}, \text{alt}, \text{time})$ is simply an average over the whole time series, $NORM(\text{lat})$ is a normalization factor and PC_i are the Principal components and the EOF_i the empirical orthogonal functions (note that these are function of spatial coordinates only).

By design the individual PC_i and EOF_i are ordered from the most “most significant” (contains the most information) to the “least significant” (contains the less information), so that truncating the series and keeping the N first EOFs will suffice to reconstruct the original signal. Therefore **this method allows to store several years of meteorological variability without having to store the huge amount of data initially produced by the model**. Nevertheless, to further limit the size of the final dataset (and also limit the size of the eigensystem to solve) the retained dataset consists of:

- Atmospheric temperature, zonal wind, meridional wind and surface pressure variables
- Fields sub-sampled on a reduced 32x24 longitude/latitude grid (half of the computational GCM 64x48 grid), and for three-dimensional quantities, on all 73 vertical levels.
- A time sampling of one data point per day, which is sufficient to reconstruct a day-to-day variability (note that the daily evolution of variables is, like the seasonal monthly evolution, already include in the MCD datasets).
- Overall, this means that a single EOF contains $32 \times 24 \times (3 \times 73 + 1) = 168960$ elements, hence the need to retain as few as possible.

Concerning the number N of EOFs suitable to retain to be able to realistically represent the original signal and its inherent variability, it is quite straightforward to test, by direct comparison between the original signal and truncated reconstructions, which value of N is sufficient. Our tests have shown that N=200 is a reasonable choice (see e.g. figure 7).

5.2.3 Reconstructing a realistic variability

Rather than reconstructing the original signal, our goal is to the original variability to recreate a realistic one (in space and time). In order to do that, one has to separate the high frequency component (ie the day-to-day variability) from the low frequency seasonal evolution. Using the fact that the temporal behavior of the decomposition is fully contained in the principal components PC_i , it is straightforward to build an alternative set of principal components which are a smoothed version (i.e. computed from the PC_i using a moving averaging windows of 30 sols) of the latter. A smoothed version of the signal, $V_{sm}(\text{lon}, \text{lat}, \text{alt}, \text{time})$ is then simply obtained as:

$$V_{sm}(\text{lon}, \text{lat}, \text{alt}, \text{time}) = AVE(\text{lon}, \text{lat}, \text{alt}) + NORM(\text{lat}) \sum_i PC_{sm\ i}(\text{time}) \times EOF_i(\text{lat}, \text{lon}, \text{alt})$$

By combining reconstructions using PC_i and $PC_{sm\ i}$ one can extract the day-to-day variations from the original signal. Similarly, one can build a new set of principal components which combine the information contained in the smoothed reconstruction and to which is added the high frequency behavior from a different (e.g. within nearby sols) instant. In practice this means that after having randomly chosen a time shift $dtime$ (which can range from -15 sols to 15 sols), a new set of principal components $PC_{new\ i}$ is generated for all times:

$$PC_{new\ i}(\text{time}) = PC_{sm\ i}(\text{time}) + [PC_i(\text{time} + dtime) - PC_{sm\ i}(\text{time} + dtime)]$$

And the perturbed series $V_{new}(\text{lon}, \text{lat}, \text{alt}, \text{time})$ is then reconstructed as:

$$V_{new}(\text{lon}, \text{lat}, \text{alt}, \text{time}) = AVE(\text{lon}, \text{lat}, \text{alt}) + NORM(\text{lat}) \sum_i PC_{new\ i}(\text{time}) \times EOF_i(\text{lat}, \text{lon}, \text{alt})$$

The key point in this procedure is that by construction the spatio-temporal coherence of transient phenomena is preserved, and that the true internal variability of the original signal is thus preserved and reproduced.

This is illustrated in figure 6 with a direct comparison, as well as in figure 7 where this time the RMS day-to-day variability of the reconstructed signal (as computed for each of the 12 Martian months, in the same way as is done in the MCD) is checked.

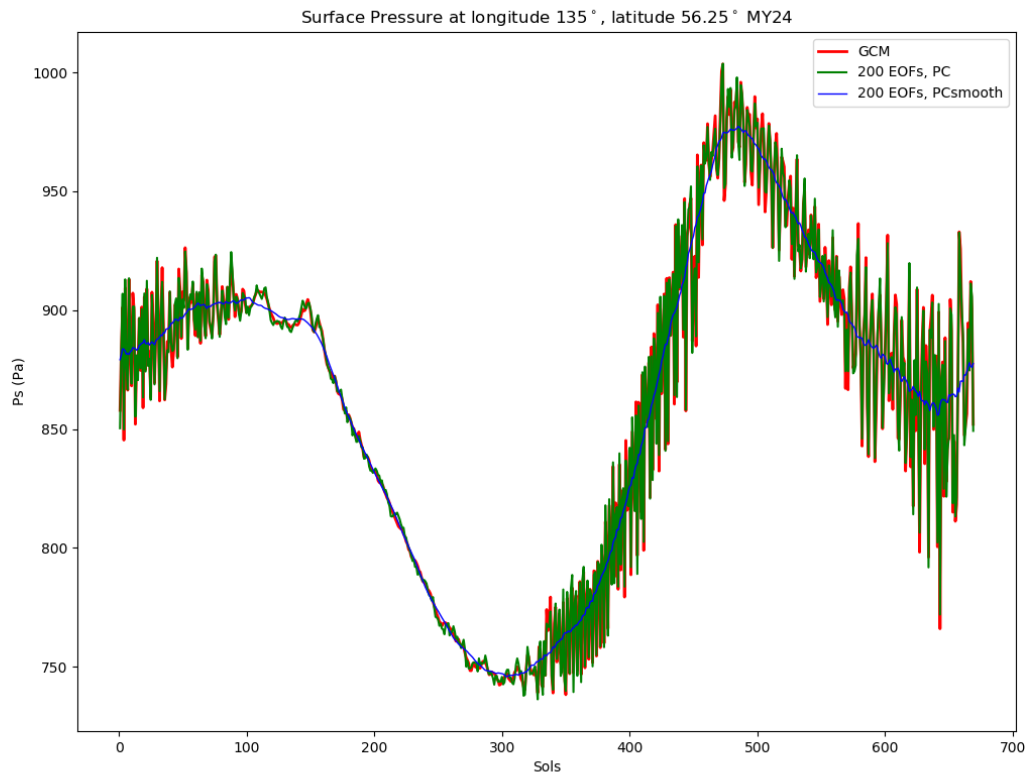


Figure 6: Example of the reconstruction of a signal (here surface pressure at a given node) with one data point per day, over one Mars year. The original signal simulated by the GCM (red) is compared to the MCD reconstruction (green) using 200 EOFs along with a reconstruction (blue) using the smoothed principal components $PC_{sm\ i}$ with which only the mean seasonal behavior is obtained.

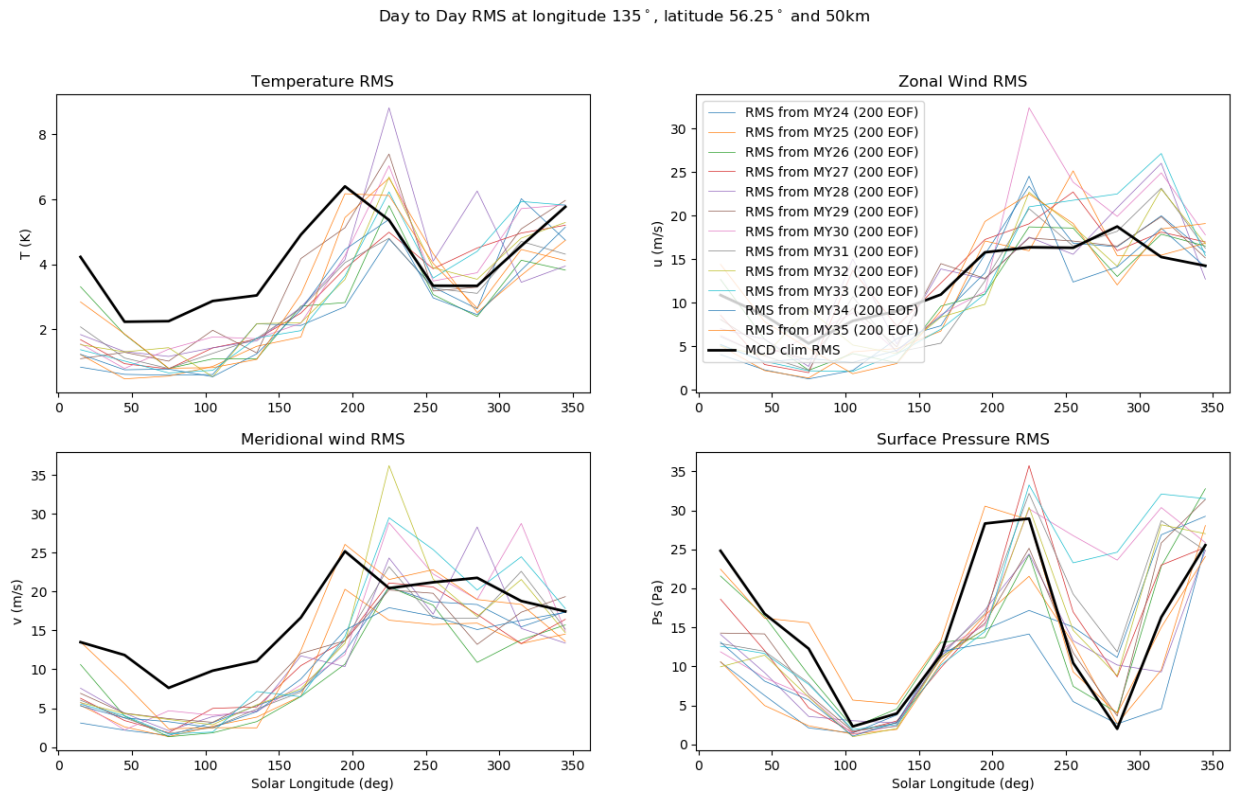


Figure 7: Example of day-to-day variability of temperature, winds and surface pressure, computed for each of the twelve martian months, using perturbed series from the large scale perturbation model. RMS values for the original GCM clim simulation (corresponding to data at lon=135 E and lat=56.25 N, close to VL2 landing site) are also displayed for comparison, along with the RMS values that are obtained using 200 EOFs

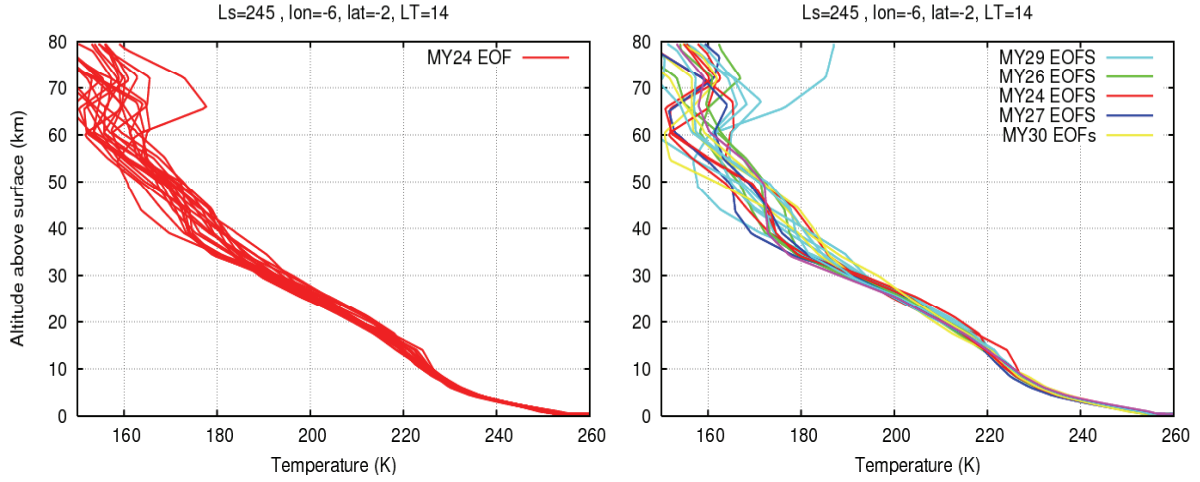


Figure 8: Illustration of the use of the MCD “large scales perturbation scheme”. Left plot: Using only the 1 year “climatology” EOFs to generate perturbed states. Right plot: using all EOF sets; note that the color codes indicate from which EOF set the perturbation was reconstructed from, but that in practice the user does not choose which EOF set is used.

5.2.4 Reconstructing the inter-annual variability of the Martian atmosphere

As mentioned above, the “mean” scenario which reflects the climatological state of the atmosphere for regular Martian years is obtained as a simulations using dust forcings corresponding to an average “standard” Mars Year. However, simulations for all regular (i.e. years without global dust storms) year have also been run (MY24, MY26, MY27, MY29, MY30, MY31, MY32, MY33). From each of these simulations, an EOF decomposition has been obtained. The improved “large scale perturbation scheme” of the MCD, when used with the “mean” scenario, uses all these sets to generate perturbed states. Repeated use of this “large scale perturbations scheme” thus give access to all the transient behaviors present in the simulations for the different Mars year, and thus offers the means to investigate the multi-annual variability of the system (figure 8).

In practice, the user doesn’t choose which EOF set is used to generate the perturbed state; switching from one EOF set to another when a new perturbation seed is provided by the user is done randomly (using that very same perturbation seed) by the MCD software

5.3 The Small-Scale Variability Model

The small-scale variability model simulates perturbations of density, temperature and wind due to the upward propagation of small-scale gravity waves. The model is based on the parameterization scheme used in the numerical models that simulated the data in the database (Forget et al., *J. Geophys. Res.* 104, 24,155-24,176, 1999)

The surface stress exerted by a vertically-propagating, stationary gravity wave can be written

$$\tau_0 = \kappa \rho_0 N_0 |\mathbf{v}_0| \sigma_0^2 \quad (23)$$

where κ is a characteristic gravity wave horizontal wave number, ρ_0 is the surface density, N_0 is the surface Brunt Väisälä frequency, \mathbf{v}_0 is the surface vector wind and σ_0 is a measure of the orographic variance. In this case we choose the model sub-grid scale topographic variance. The surface stress can be related to the gravity wave vertical isentropic displacement, δh , by

$$\tau_0 = \kappa \rho_0 N_0 |\mathbf{v}_0| \delta h^2. \quad (24)$$

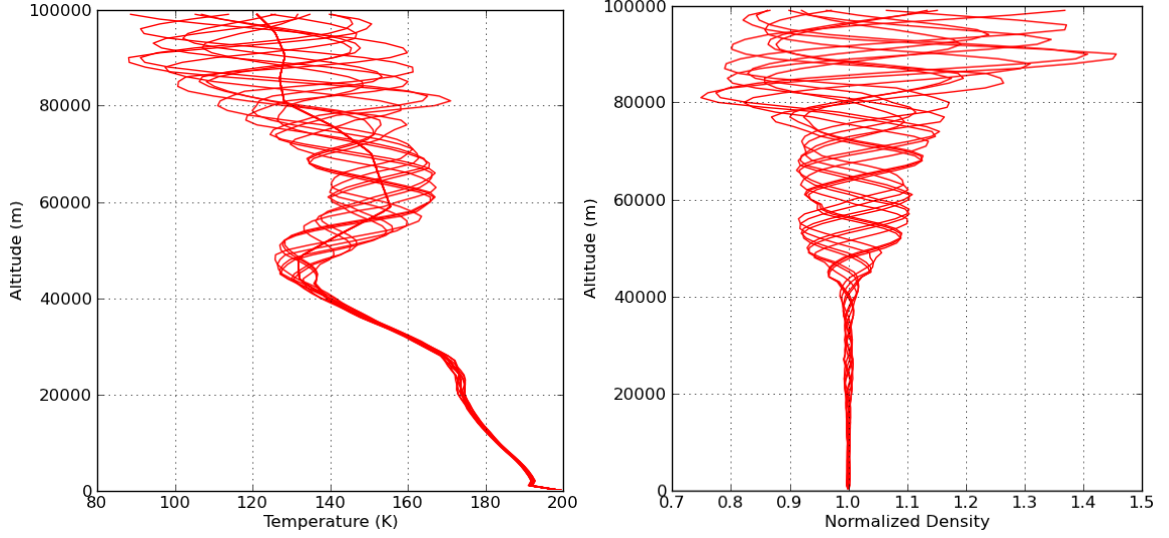


Figure 9: A series of ten perturbations, all with the same wavelength (16 km), generated by the small scale variability model added to mean profiles of temperature and density from the MCD on a vertical trajectory. Left plot: Atmospheric temperatures (including unperturbed profile). Right plot: density deviations (i.e. perturbed over unperturbed density ratios). Profiles obtained at longitude 230° East, latitude 30° South, Solar Longitude $L_s=73^\circ$ and a local time of 10 hours.

We then assume that the stress, τ , above the surface is equal to that at the surface. This leads to an expression for the wave displacement δh , at height z ,

$$\delta h = \sqrt{\frac{\rho_0 N_0 |\mathbf{v}_0| \sigma_0^2}{\rho N |\mathbf{v}|}} \quad (25)$$

where ρ , N and \mathbf{v} are the density, Brunt Väisälä frequency and wind vector at height z .

The gravity wave perturbation to a meteorological variable is calculated by considering vertical displacements of the form

$$\delta z = \delta h \sin \left(\frac{2\pi z}{\lambda} + \frac{2\pi Dist}{\lambda_{Dist}} + \phi_0 \right) \quad (26)$$

where λ is a characteristic vertical wavelength for the gravity wave, λ_{Dist} is the horizontal wavelength, such as $\lambda_{Dist} = 10 \times \lambda$, and ϕ_0 is a randomly generated surface phase angle. A set of points constituting a horizontal trajectory (varying latitude and longitude) is characterized by the dynamic distance $Dist$, representative for the wave propagation direction, and calculated between the trajectory's initial point (lat_0, lon_0) and its following points (lat, lon) (where lat and lon are respectively the latitude and longitude). $Dist$ is expressed as follows:

$$Dist = 2R_{Mars} \arcsin \left(\sqrt{\sin^2 \left(\frac{lat - lat_0}{2} \right) + \cos(lat_0) \cos(lat) \sin^2 \left(\frac{lon - lon_0}{2} \right)} \right) \quad (27)$$

The trajectory's initial point (lat_0, lon_0) remains unchanged for a complete set of points launched by the same seed, and is resaved at every new seed launch.

Perturbations to temperature, density and wind at height z are then found by using the value at $z + \delta z$ on the background profile, with the perturbations to temperature and density calculated on the assumption of adiabatic motion to the valid height.

A value can be chosen for λ , (we take $\lambda = 16$ km as a default, as it provides a reasonable comparison with the observed Viking entry temperature profiles above 50 km), in the range of 2-30 km; longer vertical wavelength should be well resolved by the model and shorter wavelengths result in negligible perturbations. By fixing the value of λ , the user will also fix the one of λ_{Dist} , such as $\lambda_{Dist} = 10 \times \lambda$, which is a

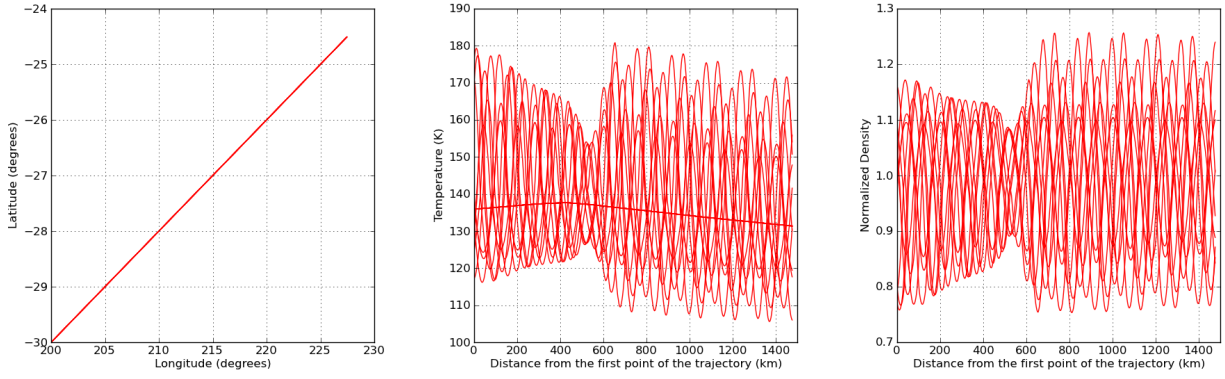


Figure 10: A series of ten perturbations, all with the same wavelength (16 km), generated by the small scale variability model added to mean profiles of temperature and density from the MCD with the example of a horizontal displacement. From left to right plot: depiction of the horizontal displacement along Latitude and Longitude; Atmospheric temperatures along the horizontal track (including unperturbed profile); Density deviations along the horizontal track (i.e. perturbed over unperturbed density ratios). Profiles obtained at altitude 80000 m, Solar Longitude $L_s=73^\circ$ and a local time of 10 hours.

realistic order of magnitude based on observations.

The amplitude of the waves, growing with the altitude, is limited by a maximum value of δz , δz_{max} , corresponding to their saturation. δz_{max} is randomly varying between $\frac{\lambda}{2\pi}$ and $3 \times \frac{\lambda}{2\pi}$, which seems reasonable according to available observations (aerobraking data from MGS, MRO, ODY, and datasets of the mass spectrometer NGIMS on board MAVEN).

An example of several small scale perturbations is shown in Figures 9 and 10 .

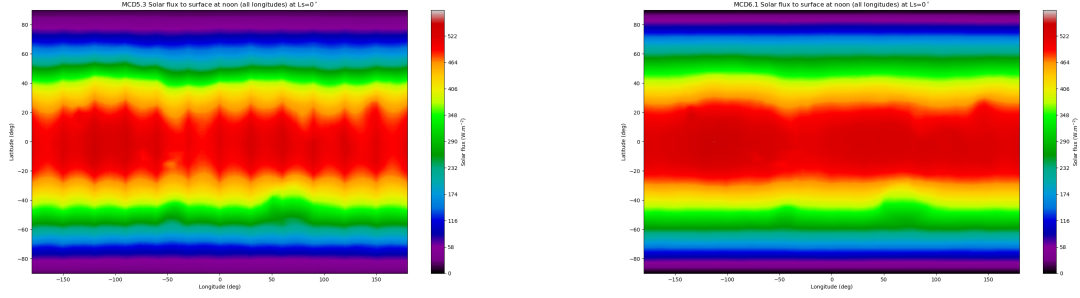


Figure 11: Solar flux to surface at noon (all longitudes) at Solar Longitude $L_s=0^\circ$, without rescaling with instantaneous solar flux (left) and with the rescaling (right)

6 Post processing of short wave fluxes

The Mars Climate Database provides several short wave fluxes :

- The incident solar flux at top of the atmosphere
- The solar flux reflected to space
- The incident solar flux on horizontal surface
- The incident solar flux on local slope at high resolution (see next section for details)
- The reflected solar flux on horizontal surface

Like all variables in the MCD, all these fluxes are monthly averaged (or calculated from monthly averaged) fields in the database and are linearly interpolated at specific location and time specified by the user in 'call_mcd' subroutine. This interpolation can make appear some unrealistic variations which are not physical at all as shown on the left pannel of Figures 11.

In order to avoid this artefact, we rescale all these short wave fluxes with the instantaneous incident solar flux at the top of the atmosphere. Therefore the MCD returns any short wave solar flux using the following equation :

$$\Phi_{SW}^{MCD}(\vec{r}, t) = \frac{\Phi_{top}^{\searrow}(\vec{r}, t)}{\bar{\Phi}_{top}^{\searrow}(\vec{r}, t)} \bar{\Phi}_{SW}(\vec{r}, t) \quad (28)$$

where $\bar{\Phi}_{SW}(\vec{r}, t)$ is any monthly mean short wave solar flux listed above from the database, $\Phi_{top}^{\searrow}(\vec{r}, t)$ is the monthly mean incident solar flux at the top of the atmosphere, also available in the database and $\bar{\Phi}_{top}^{\searrow}(\vec{r}, t)$ is the instantaneous incident solar flux at the top of the atmosphere calculated with the following equation :

$$\Phi_{top}^{\searrow}(\vec{r}, t) = \frac{F_{1AU}}{D_{SM}^2(t)} \mu_0(\vec{r}, t) \quad (29)$$

with μ_0 the cosine of the solar zenith angle, $F_{1AU} = 1370 \text{ W.m}^{-2}$ the solar constant which represents the solar flux at one astronomical unit, D_{SM} the distance Sun-Mars in astronomical unit. As it can be seen on the right panel of Figures 11, this rescaling allows to remove the unrealistic variations due to the temporal interpolation between monthly mean fields.

7 High Resolution Outputs

The Mars Climate Database has been compiled from the output of a general circulation model in which the topography is very smoothed because of its low resolution. In addition, the pressure variations due to the CO₂ cycle (condensation of atmospheric CO₂ in the polar caps) that is computed by the model is only based on the simulation of the actual physical processes. The polar cap physical properties have been tuned somewhat to reproduce the observations, but no correction was added.

The access software includes a “high resolution” mode which combines high resolution (32 pixels/degree) MOLA topography and the smoothed InSight pressure records (used as a reference to correct the atmospheric mass) with the MCD surface pressure in order to compute surface pressure as accurately as possible. The latter is then used to reconstruct vertical pressure levels and hence, within the restrictions of the procedure, yield high resolution interpolated values of atmospheric variables.

All these post-processing procedures are detailed in the following subsections.

7.1 High Resolution Topography and Areoid

The MCD includes (and uses) topography and areoid (Mars geoid) at the database’s resolution (64×49 in longitude \times latitude). The need to yield higher resolution outputs has led to the development of post-processing tools which require knowledge of these two fields at a much higher resolution. This is achieved using the most up-to-date models and datasets distributed by the Mars Orbiter Laser Altimeter (MOLA) Team.

7.1.1 Mars Gravity Model

Very high resolution values of the Martian areoid can be computed using the MGM1025 spherical harmonic solution of the Mars gravity field to degree and order 80, using X band tracking data of the MGS Mars Orbiter Laser Altimeter. This model is an update of the Goddard Mars Model 2B (GMM2B) described in Lemoine et al. (*J. Geophys. Res.*, 106(E10), 2001) and follows the IAU2000 rotation model and cartographic frame (see Seidelmann et al., *Cel. Mech. Dyn. Astron.*, 82, 83-110 2002) recommended by the Mars Cartography Working Group.

A Fortran program to compute the radius of the geoid at given areocentric latitude and longitude, along with a file containing the MGM1025 coefficients, are kindly made available by G. Neumann from: <http://ltpwww.gsfc.nasa.gov/tharsis/data.html>

The supplied `areoid.f` program was adapted and merged into the MCD `heights.F` collection of routines which uses the MGM1025 gravity field coefficients (file `mgm1025` in `data` directory of the MCD obtained from the same source. From version 6.1, this tool is now included inside the `MCD.F90` module.

7.1.2 MOLA Topography

The MOLA Precision Experiment Data Record (PEDR) are archived and distributed by the Planetary Data System (<http://pds.jpl.nasa.gov>) and include topography data binned at various resolutions (from 4 pixels per degree to 128 pixels per degree for the whole planet and up to 512 pixels per degree in the polar regions).

The 32 pixel per degree topography file (a binary file) was converted to NetCDF, yielding the ‘`mola32.nc`’ file (in the `data` directory of the MCD) which is used by MCD software. The choice of this resolution as “high resolution” results from a compromise between datafile size and need for resolution (32 pixels per degree corresponds to a 1850 m resolution at the equator, where the mesh is largest); the file `mola32.nc` is already a 127 Mb file (a higher resolution 64 pixels per degree topography file would be 4 times bigger, i.e. around 520 Mb).

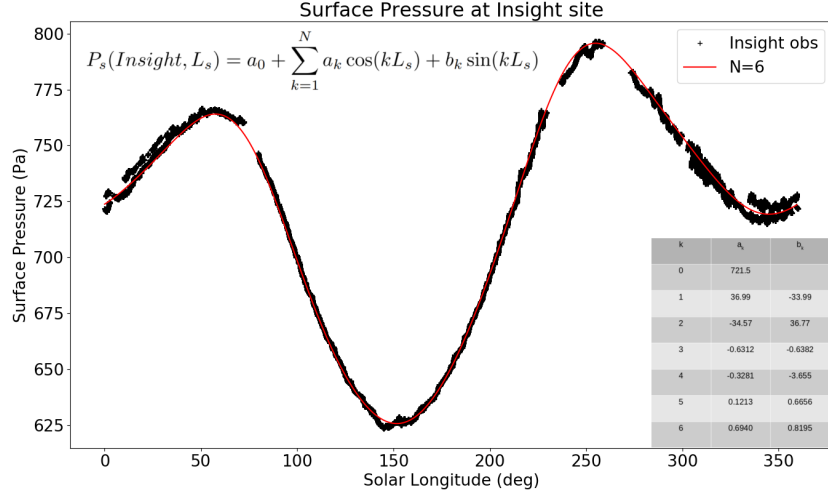


Figure 12: Smoothed InSight surface pressure records with Fourier series (6 harmonics).

7.2 Deriving High Resolution Surface Pressure

High resolution surface pressure may be obtained from GCM surface pressure by using InSight records to correct atmospheric mass and by taking into account the change in altitude from the (coarse and smoothed) GCM topography to more realistic high resolution topography.

In practice, an estimation of the high resolution surface pressure P_s at a given location and time is given by:

$$P_s = P_{s_{\text{GCM}}} \frac{\langle P_{\text{InsObs}} \rangle}{\langle P_{\text{InsGCM}} \rangle} e^{-(z-z_{\text{GCM}})/H} \quad (30)$$

where $P_{s_{\text{GCM}}}$ is the pressure predicted by the GCM at the same location and time (bilinear interpolations from the MCD grid), $\langle P_{\text{InsObs}} \rangle$ the InSight surface pressure records smoothed to remove thermal tides and transient waves, $\langle P_{\text{InsGCM}} \rangle$ the similarly smoothed (i.e. diurnally averaged) InSight surface pressure predicted by the GCM (interpolated vertically and horizontally), z is the altitude of the local surface retrieved from the MOLA dataset, and z_{GCM} is the altitude at the location interpolated from the coarse GCM topography grid. H is the scale height used in the hydrostatic equation to vertically interpolate the pressure: $H = RT/g$ with R ($\text{m}^2 \text{s}^{-2} \text{K}^{-1}$) the gas constant, $g = 3.72 \text{ m s}^{-2}$ the acceleration of gravity, and T the atmospheric temperature extracted from the GCM at about 1 km above the surface⁷. The choice of this altitude to interpolate surface pressure on Mars is based on the theoretical considerations and tests described in Spiga et al. (*J. Geophys. Res.*, 112, E08S16, 2007).

The smoothed InSight surface pressure records is computed using Fourier series of the observations from InSight. It was chosen to keep 6 harmonics in order to represent 1 month variations maximum. The coefficients of these harmonics and the comparison with the observations are presented on Figure 12.

This procedure to predict high resolution surface pressure was initially provided with Mars Climate Database version 4.1, as a distinct external tool, ‘pres0’. Since version 4.2 and 5. of the MCD, the main routine ‘call_mcd’ can yield high resolution outputs and uses the procedure described above to derive high resolution surface pressure values. Therefore the ‘pres0’ tool is no more provided as a standalone tool.

An example of the impact of the high resolution scheme is given in Figure 13 where are plotted the surface pressure, at GCM resolution, at InSight site along with the pressure (at the same elevation) that is obtained (see next section) from the high resolution surface pressure derived using the scheme described above. Note that due to the “total atmospheric mass correction” term, the $\langle P_{\text{InsObs}} \rangle / \langle P_{\text{InsGCM}} \rangle$ ratio

⁷Technically, the temperature that is used is that of the 7th atmospheric layer, which is located at about 1 km above the surface (see Section 2.4.2).

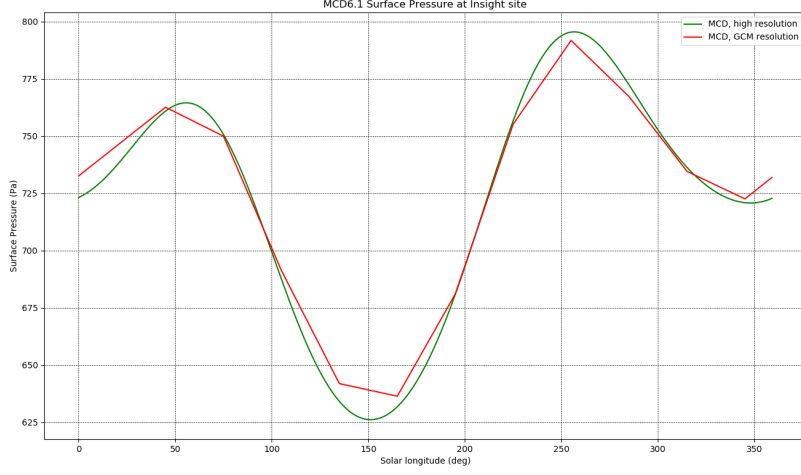


Figure 13: Illustrative example of the effect of the high resolution mode: Pressure at InSight location (longitude 135.62345° east and latitude 4.50238° north)

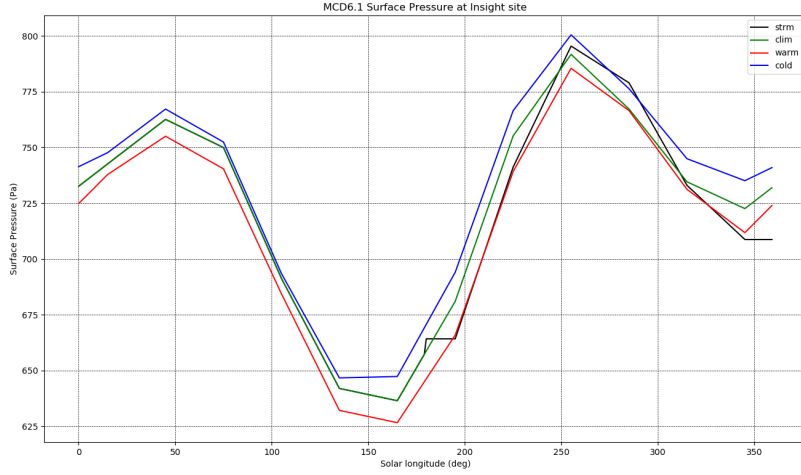


Figure 14: Effect of the dust storm case scenario on the surface pressure predicted by the MCD at InSight site

in Eq. 30, the difference between GCM resolution and high resolution pressures at a fixed location varies non-monotonically with solar longitude.

As the InSight pressure cycle is not altered by the dust conditions (see Figure 14), no specific treatment is needed for dust storm case and InSight pressure records can be used as reference for all scenarios.

7.3 Computing High Resolution Values of Atmospheric Variables

7.3.1 Interpolation of Atmospheric Temperature

The MCD contains the atmospheric temperatures obtained from the corresponding GCM runs, on the same grid (as described in Section 2.4), and thus at given pressure $P(l)$ for a given location and layer l (computed from surface pressure $P_{s_{GCM}}$ interpolated from the 3.75° latitude by 5.625° longitude 64×73 MCD grid, using Equation 1 as shown in Section 2.4.2). If, however, the surface pressure should in fact be $P_{s_{HR}}$, as given by Equation 30, then a legitimate question is then: How should the atmospheric

temperature profile $T(l)$ above $P_{s_{HR}}$ be interpolated?

To better understand this issue, i.e. the behavior of atmospheric temperature field over topography at higher resolutions, high resolution simulations (176×132 at LMD and up to 512×256 at The Open University) were performed and their output compared to the lower (64×49) resolution ones.

These simulations show that temperature behaves as follows :

1. When topography -and thus surface pressure- varies locally, surface temperature is not affected (it is in radiative equilibrium; only the variation of dust opacity affects the surface temperature, but the impact should be small compared to the variations of albedo, thermal inertia, and slope).
2. To first order, temperature near the surface (first few kilometres) is controlled by the distance from the surface. Above, it is controlled by the pressure level, somewhat independently from the kilometre scale topography.
3. To second order, the near surface air temperature is colder in high altitude regions than in the neighbouring plains, as a result of adiabatic cooling.
4. In local depressions (crater, canyon, etc..), the opposite effect is observed (near surface air warming) but it is less significant.

These facts are taken into account to build the rules to use to interpolate temperature in “high resolution” mode: The MCD temperature profile $T(l)$ is not changed, but the corresponding pressure levels $P(l)$ are. Doing so moreover enables the use of the same database access software as with the “low resolution”, except for the adjustment of pressure levels.

After a bit of tuning and applying rules 1 to 4 above, it has been found that the new “high resolution” pressure levels $P_{HR}(l)$ can be built using a function designed to ensure a smooth transition from the near-surface conditions to the free atmosphere (high altitude) environment:

$$P_{HR}(l) = P_{GCM}(l) [f(l) + (1 - f(l)) 0.5 (1 + \tanh(6 (-10 \ln(\frac{P_{GCM}(l)}{P_{s_{GCM}}}) - z)/z))] \quad (31)$$

where $P_{GCM}(l)$ is the original pressure level in the database. z roughly corresponds to the altitude above the surface (in the GCM smoothed topography) where P_{HR} will become equal to P_{GCM} . It varies depending on the altitude difference (derived from pressure) between the high and low resolution grid Δz (km) :

$$\Delta z = -10 \ln \left(\frac{P_{s_{HR}}}{P_{s_{GCM}}} \right) \quad (32)$$

And z is set to:

$$\begin{aligned} z &= \Delta z + 3 \text{ if } \Delta z > 0 \text{ (local mountain)} \\ z &= 3 \text{ if } \Delta z < 0 \text{ (local depression)} \end{aligned}$$

$f(l)$ is a variable parameter which is equal to 1 at high altitude (then $P_{HR}(l) = P_{GCM}(l)$). At low altitude, it is designed to ensure that the first levels will be at the same distance from the surface in both low and high resolution (then $P_{HR}/P_{s_{HR}} = P_{GCM}/P_{s_{GCM}}$ except when there is a local high topography structure (HR surface more than 1 km above the GCM surface). In such conditions the model levels are compressed closer to the surface, to mimic the observed behaviour in high resolution GCM simulations. Conversely the model levels are expanded when there is a topographic low. (HR surface more than 1 km below the GCM surface). In practice $f(l)$ is computed as:

$$f(l) = \frac{P_{s_{HR}}}{P_{s_{GCM}}} \left(\frac{P_{GCM}(l)}{P_{s_{GCM}}} \right)^x \quad (33)$$

where x is the parameter which control the compression of the extension of the layers near the surface (no effect when $x = 0$, compression if $x < 0$, extension if $x > 0$).

The value of x is derived from that of Δz :

$$\begin{aligned}
x &= 0 && \text{if } -1 < \Delta z < 1 \\
x &= -0.12 (|\Delta z| - 1) && \text{if } \Delta z > 1 \\
x &= +0.12 (|\Delta z| - 1) && \text{if } \Delta z < -1 \\
x &= 0.8 && \text{if formulas above yield } x > 0.8 \\
x &= -0.8 && \text{if formulas above yield } x < -0.8
\end{aligned}$$

Figures 15 and 16 display examples of the temperature fields produced by the “high resolution” MCD V4.2 compared to the “low resolution” version and true high resolution (176×132) GCM output.

7.3.2 Interpolation of Density

In the low resolution version of the database, the density ρ (kg m^{-3}) at altitude z (m) is interpolated in the vertical by using a weighted interpolation between the density at the level above (ρ_{l+1}) and the density at the level below (ρ_l). In practice the linear interpolation is performed on the logarithm of the density (as mentioned in Section 4.2.2).

Density is proportional to pressure and thus, in the “high resolution” mode, it must be recomputed by taking into account the change in pressure (computed using Equation 31). The algorithm for vertical interpolation that is used for “low resolution” density is used to compute “high resolution” density, but using $\rho_{l+1} P_{\text{HR}}(l+1)/P_{\text{GCM}}(l+1)$ and $\rho_l P_{\text{HR}}(l)/P_{\text{GCM}}(l)$ instead of ρ_{l+1} and ρ_l .

A similar treatment is applied to the RMS of density, corresponding perturbations, etc...

7.3.3 Modification of Other Variables

Most other atmospheric variables X (winds, turbulent kinetic energy, gases and ice mixing ratio) are treated like temperature: the values of the profile $X(l)$ are kept, and only the pressure of the levels $P(l)$ are recomputed to account for the “high resolution” post-processing.

The dust optical depth τ is scaled to the high resolution surface pressure (e.g. $\tau_{\text{HR}} = \tau_{\text{GCM}} P_{\text{S}_{\text{HR}}}/P_{\text{S}_{\text{GCM}}}$).

Column densities properly integrated in low resolution are already stored in the MCD data files. In order to get columns for the high resolution surface pressure, the two columns are roughly integrated over high and low resolution sigma levels based on the hydrostatic equation:

$$\begin{aligned}
c_{\text{GCM}}^j &= \sum_{l=2}^{l=L} \{ (\text{vmr}^j(l) R_m(l) [P_{\text{GCM}}(l-1) - P_{\text{GCM}}(l)] / (g_m(l) k_b) \} \\
c_{\text{HR}}^j &= \sum_{l=2}^{l=L} \{ (\text{vmr}^j(l) R_m(l) [P_{\text{HR}}(l-1) - P_{\text{HR}}(l)] / (g_m(l) k_b) \}
\end{aligned} \tag{34}$$

where vmr^j is the volume mixing ratio of specie j , k_b is the Boltzmann constant. Then to scale to the high resolution surface pressure the low resolution column density from the MCD data files is multiplied by the ratio $c_{\text{HR}}/c_{\text{GCM}}$.

7.4 Computation of the solar irradiance on the surface

7.4.1 Computation of the slope inclination and orientation

An evaluation of the inclination and the orientation of the slope is necessary to compute the solar irradiance on the slope. In order to calculate the inclination α and the orientation ψ of the slope on a given point $M(lon, lat)$ at longitude lon and latitude lat on the Martian surface, we built an equilateral triangle ABC , where each point is distant from M by a distance p , as shown on Figure 17.

Therefore the coordinates of each point A , B and C are given by the following equations :

$$\begin{cases} lat_A = lat + p/R_c \\ lat_B = lat - p/(2R_c) \\ lat_C = lat - p/(2R_c) \end{cases} \tag{35}$$

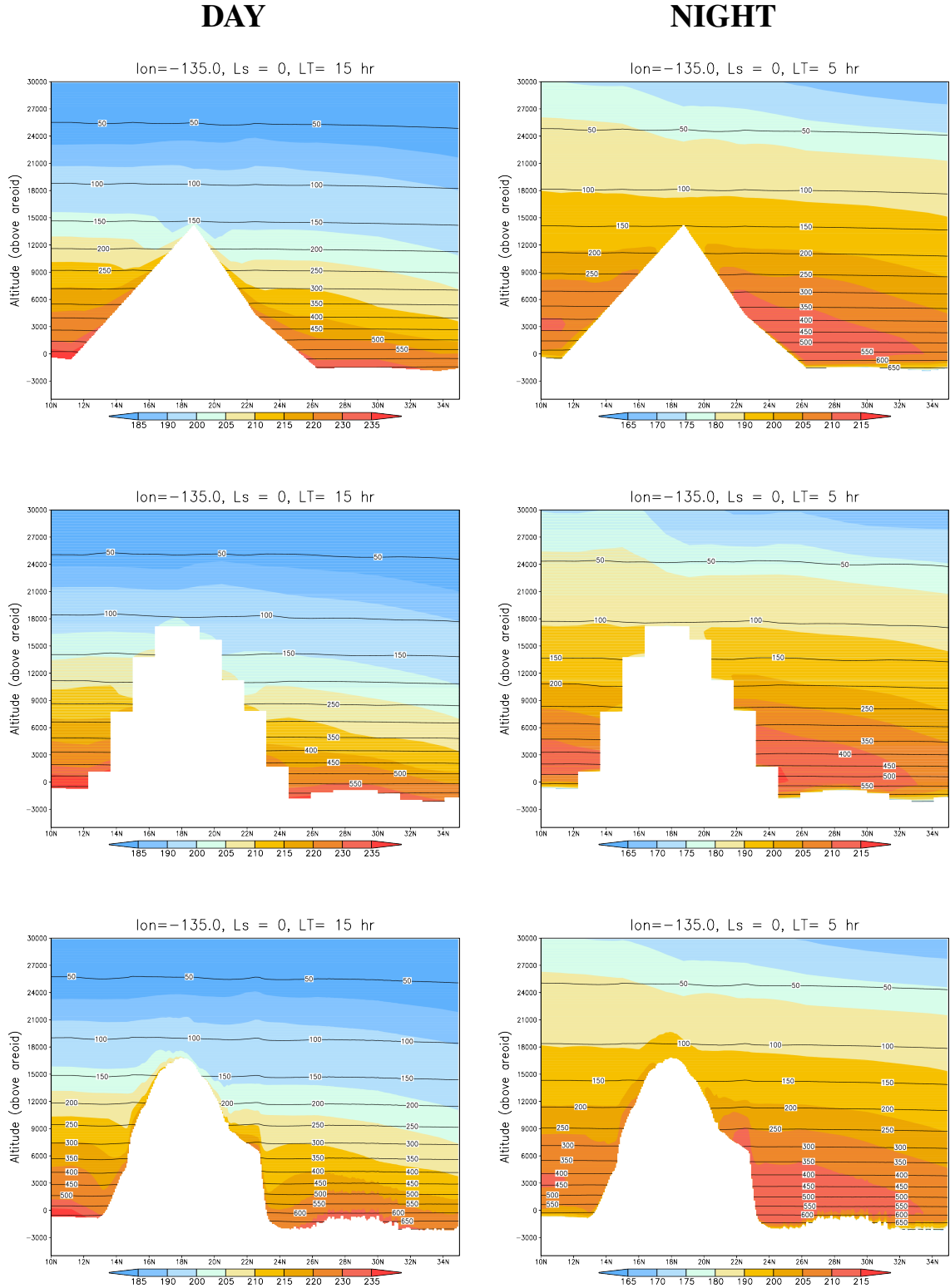


Figure 15: Cross-section of temperature fields (colored) and pressure level (black contour) near Olympus Mons from the MCD at GCM resolution (top row), from a high resolution 176×132 GCM run (middle row), and from the high resolution output of the MCD (bottom row). Note that there is an order of magnitude between horizontal and vertical scales in these plots; what appear as sharp gradients in the horizontal direction are in fact quite smooth when displayed using more commensurate axes.

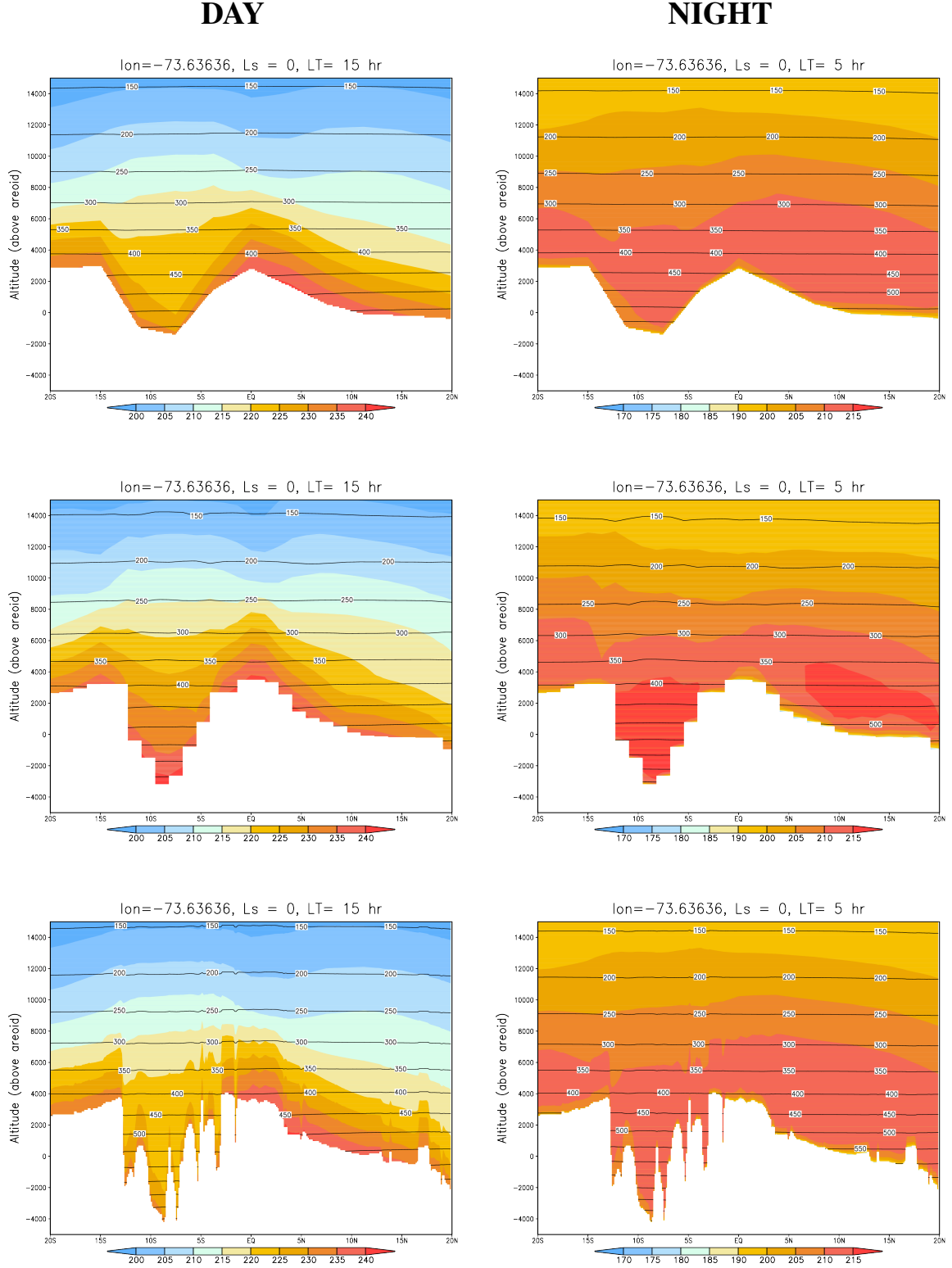


Figure 16: Cross-section of temperature fields (colored) and pressure level (black contour) near Valles Marineris from the MCD at GCM resolution (top row), from a high resolution 176×132 GCM (middle row), and from the high resolution output of the MCD. Note that there is an order of magnitude between horizontal and vertical scales in these plots; what appear as sharp gradients in the horizontal direction are in fact quite smooth when displayed using more commensurate axes.

$$\begin{cases} \text{lon}_A = \text{lon} \\ \text{lon}_B = \text{lon} + \sqrt{3}p/(2R_c \cos(\text{lat}_B)) \\ \text{lon}_C = \text{lon} - \sqrt{3}p/(2R_c \cos(\text{lat}_C)) \end{cases} \quad (36)$$

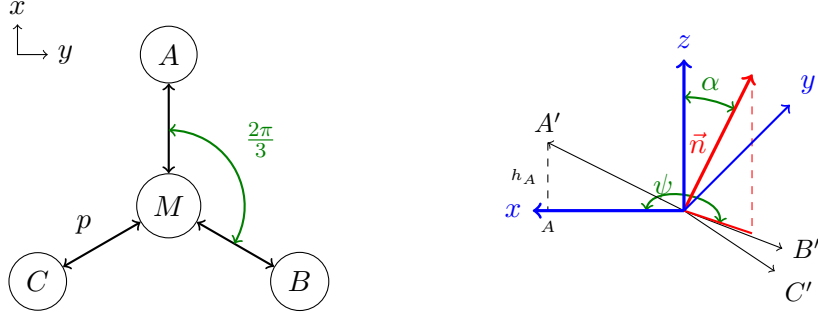


Figure 17: Three points calculation of the slope. On the left, the initialization of the points. On the right, the definition of the variables. (M) is the desired location, we set (A), (B) and (C) such as their distance from (M) equals p , and for them to be forming an equilateral triangle.

where R_c is the distance of M from the center of the planet and coordinates being expressed in radians. Once the triangle is built, one can find the real altitude of the points A , B and C , denoted respectively as h_A , h_B and h_C , interpolated with the NetCDF file mola.nc containing the high resolution topography of Mars as a function of the longitude and the latitude. This gives us three new points A' , B' and C' .

Let $\vec{v} = \begin{pmatrix} a \\ b \\ c \end{pmatrix} \in \mathbb{R}^3$ an orthogonal vector of the plane defined by the three points $A'(lon_A, lat_A, h_A)$, $B'(lon_B, lat_B, h_B)$ and $C'(lon_C, lat_C, h_C)$. Every point (x, y, z) of this tangent surface has to be a solution of the following equation:

$$ax + by + cz + d = 0 \quad (37)$$

with $d \in \mathbb{R}$.

We apply this equation with $d = 0$ to A' , B' and C' which Cartesian coordinates can be written as follows :

$$\begin{cases} x_A = x_M + p \\ x_B = x_M - p/2 \\ x_C = x_M - p/2 \end{cases} \begin{cases} y_A = y_M \\ y_B = y_M + p\sqrt{3}/2 \\ y_C = y_M - p\sqrt{2}/2 \end{cases} \begin{cases} z_A = h_A \\ z_B = h_B \\ z_C = h_C \end{cases} \quad (38)$$

where x_M and y_M define the coordinates of M in the Cartesian coordinate system.

Therefore we obtain three equations which lead to two independent equations :

$$\begin{cases} a = \frac{h_B + h_C - 2h_A}{3p}c \\ b = \frac{h_C - h_B}{\sqrt{3}p}c \end{cases} \quad (39)$$

We can choose to set $c = 3p$, then :

$$\vec{v} = \begin{pmatrix} h_B + h_C - 2h_A \\ \sqrt{3}(h_C - h_B) \\ 3p \end{pmatrix} \quad (40)$$

The unit vector \vec{n} is set as $\vec{n} = \frac{\vec{v}}{\|\vec{v}\|}$. Knowing that $\cos(\alpha) = \vec{n} \cdot \vec{e}_z$, then

$$\cos(\alpha) = \frac{1}{\sqrt{1 + \left(\frac{2}{3p}\right)^2 (h_A^2 + h_B^2 + h_C^2 - h_A h_B - h_A h_C - h_B h_C)}} \quad (41)$$

Considering an orientation of the slope ψ null if the slope is oriented northward (towards \vec{e}_x direction) and 90° eastward (towards \vec{e}_y direction), we have $\tan(\psi) = (\vec{n} \cdot \vec{e}_y) / (\vec{n} \cdot \vec{e}_x)$:

$$\tan(\psi) = \sqrt{3} \frac{h_C - h_B}{h_B + h_C - 2h_A} \quad (42)$$

We have therefore the following final expressions for the slope inclination α and the slope orientation ψ :

$$\alpha = \arccos \left(\left(\sqrt{1 + \left(\frac{2}{3p} \right)^2 (h_A^2 + h_B^2 + h_C^2 - h_A h_B - h_A h_C - h_B h_C)} \right)^{-1} \right) \quad (43)$$

Or in an equivalent way :

$$\alpha = \arctan2 \left(2\sqrt{h_A^2 + h_B^2 + h_C^2 - h_A h_B - h_A h_C - h_B h_C}, 3p \right) \quad (44)$$

and the orientation is computed as follows

$$\psi = \arctan2(\sqrt{3}(h_C - h_B), h_B + h_C - 2h_A) \quad (45)$$

where $\arctan2(y, x)$ is defined as the angle between the positive x axis and the ray to the point (x, y) .

The parameter p was set to $p = 2 \text{ km}$, i.e. around the MOLA resolution, in order to avoid the points A' , B' and C' to 'fall' several times in craters which would make each element of the topography appear several times on the maps.

7.4.2 Computation of the solar irradiance on the slope

A method of computation of the solar irradiance is set out in *Spiga et al.* (2008). The total solar irradiance F on a given unit surface on a slope is given by :

$$F = D + S + R \quad (46)$$

where D is the direct incoming flux from the Sun, S is the scattered flux by the dust and R is the reflected flux from the surrounding terrains. The fluxes on a Martian horizontal surface are written F_0 , D_0 and S_0 .

The scattered and reflected flux on an horizontal surface are computed from the total solar irradiance on an horizontal surface which is available in the database of the MCD. However the direct incoming flux on an horizontal surface is computed as follows :

$$D_0 = \frac{F_{1AU}}{D_{SM}^2} \mu_0 \exp \left(-\frac{\tau_{dust} + \tau_{cloud}}{\mu_0} \right) \quad (47)$$

with μ_0 the cosine of the solar zenith angle, $F_{1AU} = 1370 \text{ W.m}^{-2}$ the solar constant which represents the solar flux at one astronomical unit, D_{SM} the distance Sun-Mars in astronomical unit, τ_{dust} the dust optical depth and τ_{cloud} the opacity of ice clouds. The latter is computed as follows :

$$\tau_{cloud} = \frac{3M_{ice}Q_{ext}}{4\rho_{ice}r_{eff}} \quad (48)$$

with M_{ice} the column area density of ice, $Q_{ext} = 2$ the single scattering extinction coefficient, $\rho_{ice} = 920 \text{ kg.m}^{-3}$ the ice density and $r_{eff} = 5 \text{ }\mu\text{m}$ the cloud particle effective radius.

The direct incoming flux is given by

$$D = \frac{\mu_s}{\mu_0} D_0 \quad (49)$$

where μ_s is the cosine of the angle between the incident Sun rays and the normal of the slope such as

$$\mu_s = \max[0, \mu_0 \cos(\alpha) + \sqrt{1 - \mu_0^2} \sin(\alpha) \cos(\psi - \psi_0)], \quad (50)$$

with μ_0 the cosine of the solar zenith angle and ψ_0 the solar azimuth.

Concerning the reflected flux, it can be calculated under the assumption of Lambertian surface with albedo A_L :

$$R = (1 - \sigma_s) A_L (D_0 + S_0) \quad (51)$$

where

$$\sigma_s = \frac{1}{2} (1 + \cos \alpha) \quad (52)$$

is called the sky-view factor.

Finally, the scattered flux is

$$S = S_0 s^t \times (M + \mu_0 N) \times g \quad (53)$$

where

$$s = \begin{bmatrix} 1 \\ \exp(-\tau_{dust}) \\ \sin(\alpha) \\ \exp(-\tau_{dust}) \sin(\alpha) \end{bmatrix}, \quad g = \begin{bmatrix} \frac{\mu_s}{\mu_0} \\ 1 \end{bmatrix}. \quad (54)$$

M and N are two 4×2 coupling matrices empirically determined in *Spiga et al.* (2008) with a reference Monte-Carlo radiative transfer code.

An example of what can be obtain with the MCD using this method is shown in Figure 18. This Figure shows the total irradiance at Valles Marineris site at 8am, at a solar longitude of $L_s = 0^\circ$. Comparatively, there is a picture of Valles Marineris made by the Viking orbiter.

To fully validate our model, the MCD was also compared to the validated LMD1D model (version 4) which also computes the solar irradiance on the Martian surface. However in the LMD1D model, the slope inclination and orientation are given by the user as inputs of the simulation, just like surface pressure. Therefore we chose some locations on Mars and observed the slope inclination and orientation, the surface pressure returned by the MCD, we used these values as inputs of the LMD1D model and compared the solar irradiance received by the surface along one full day at different solar longitudes.

The comparisons were done at different locations. Figure 19 shows one of these comparisons at Olympus Mons site with the 'Climatology' scenario for dust opacity . We can see that we have a good fit for both comparisons. However when the cosine of the solar zenith angle approaches zero, we observe a slight gap between the two models before that the MCD solar irradiance model falls to zero. This is due to the fact that the reflected and scattered solar flux are computed in the MCD from the total solar flux on an horizontal surface. But this latter flux is taken from the database which is, like every field, averaged over several months. On the contrary, in the LMD1D model , the instantaneous flux is used. This is why, when the cosine of the solar zenith angle is under an arbitrary value that we decided to set to 0.01, we force the solar irradiance on the slope to 0 $W.m^{-2}$. This explains the form of the figures obtained.

7.5 Computation of high resolution slope winds

7.5.1 The model

The model used is the one developed by Prandtl in *Prandtl et al.* (1942) :

$$\begin{cases} \frac{\partial}{\partial z} \left(K \frac{\partial u}{\partial z} \right) + f v + f_b = 0 \\ \frac{\partial}{\partial z} \left(K \frac{\partial v}{\partial z} \right) - f u = 0 \end{cases} \quad (55)$$

with the upslope flow u and the cross-slope wind v , the eddy coefficient K , and the Coriolis parameter f . f_b represents the buoyancy force such that :

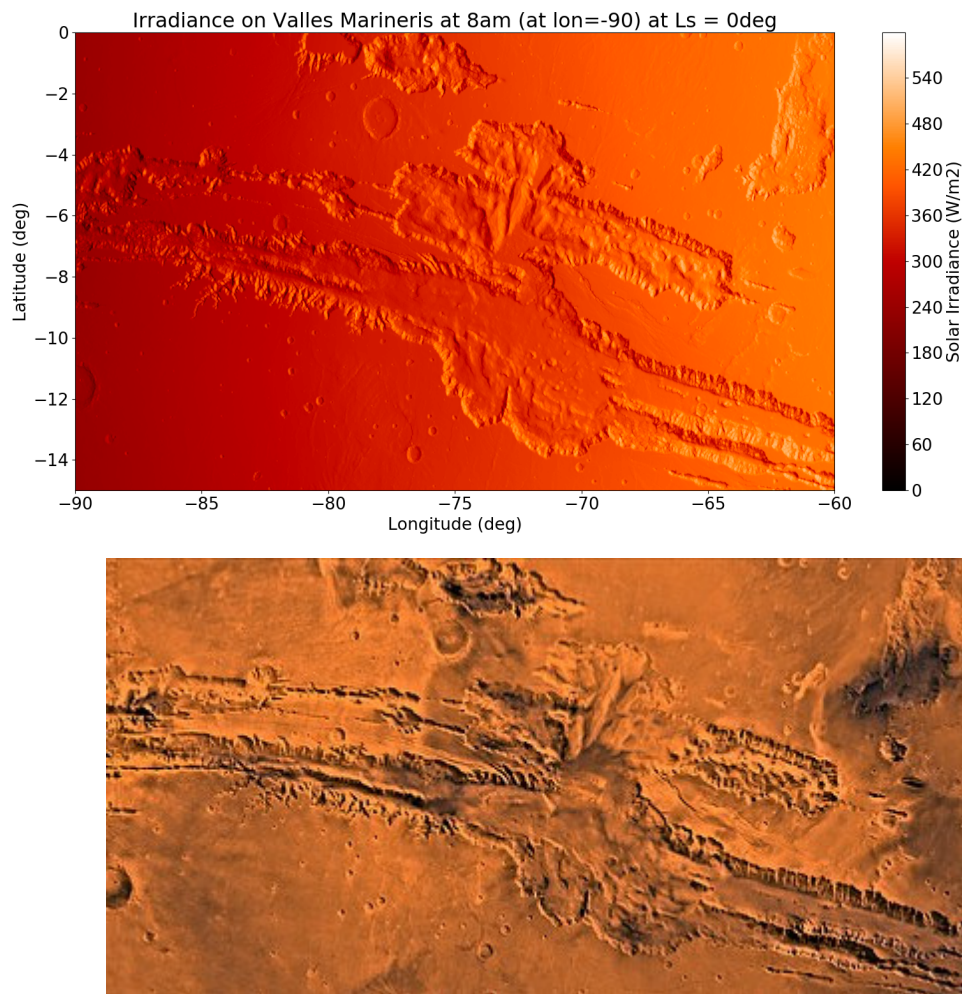


Figure 18: Maps of solar irradiance ($W.m^{-2}$) computed from the MCD in Valles Marineris site at the top. The local times at longitude -90° is 8 a.m. At the bottom, Image of Valles Marineris made by Viking orbiter, Image Credit: NASA/JPL/USGS.

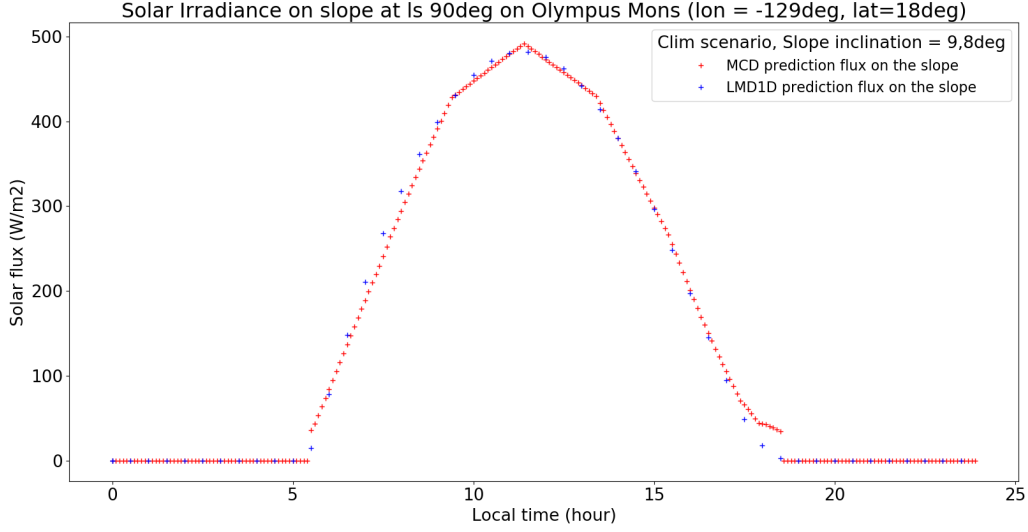


Figure 19: Solar irradiance on slope at Olympus Mons site at $L_s = 90^\circ$ with 'Climatology' scenario for the LMD1D model (in blue) and the MCD (in red)

$$f_b(z) = \frac{\theta(z) - \theta_0}{\theta_0} g \sin \alpha \quad (56)$$

with g the Martian acceleration of gravity, α the inclination of the slope, θ the potential temperature and θ_0 the background potential temperature at the same height.

7.5.2 Calculation of the slope inclination and orientation to compute slope winds

The large scale wind being already stored in the database and since we are only interested here in modelling small scale slope winds, we calculate the wind on a specific high resolution topography which corresponds to the difference between MOLA topography and GCM topography.

Then the same method as the one described in section 7.4.1 is used to compute slope inclination and orientation, only with three triangles instead of one and at a resolution of $p = 10 \text{ km}$. We denote by α_{loc} and ψ_{loc} respectively the slope inclination and the slope orientation calculated with this method. Then in order to consider very strong slope near the considered point that will create slope wind and that is not modeled by the equations of our model, we do not consider α_{loc} and ψ_{loc} in our equations but α and ψ such that :

$$\begin{cases} \alpha(M) = \max_{\{x,y\} \in \mathcal{C}(M,R)} \left\{ \alpha_{\text{loc}}(x,y) \left(1 - \frac{d(x,y)}{R} \right) \right\} \\ \psi(M) = \psi_{\text{loc}} \left(\arg \max_{\{x,y\} \in \mathcal{C}(M,R)} \left\{ \alpha_{\text{loc}}(x,y) \left(1 - \frac{d(x,y)}{R} \right) \right\} \right) \end{cases} \quad (57)$$

where $\mathcal{C}(M, R)$ is the circle with center M and radius R and $d(x, y)$ is the distance between M and the point of coordinates (x, y) . This allows to take into account the influence of near strong slopes on the local slope wind. We want to consider this influence at a few tens km, that is why it was chosen to set $R = 40 \text{ km}$.

The two fields $\alpha(x, y)$ and $\psi(x, y)$ are stored in the database in the file 'slope_map.nc'.

7.5.3 Buoyancy term

Once the user has chosen a location the software has only access to the fields in the considered column of atmosphere. The buoyancy term depending on the potential temperature θ_0 of the atmosphere not influenced by the slope at the same altitude above reference areoid, the temperature on an other column is necessary to compute this term. This is why instead of using directly this temperature θ_0 , we assume that it is equal to the temperature in the considered column at a higher altitude. Indeed, the surface influences the atmosphere in the first kilometers near the slope and therefore the isotherms follow the topography as shown on Figure 16. So θ_0 is replaced by :

$$\theta_0 = \theta(z + \Delta z) \quad (58)$$

However as the altitude becomes higher the temperature is less and less influenced by the slope until we have $\theta_0 = \theta(z)$. Therefore Δz must be a function of the altitude above the surface z , that decreases with altitude until reaching zero at a given limit altitude and stays null above this limit altitude called z_{lim} . Above around $z_{\text{lim}} = 500\text{m}$, temperature is not influenced by the topography anymore. For the sake of simplification, it was chosen to make Δz decrease linearly with z , choosing $\Delta z(0) = H_{\text{PBL}} \sin \alpha$ where H_{PBL} is the convective Planetary Boundary Layer (PBL). During night the PBL height can become very low, reaching at some hours zero, therefore we limit its value to a minimum of $z_{\text{min}} = 80\text{m}$.

$$\forall z \in [0, z_{\text{lim}}], \Delta z(z) = H_{\text{PBL}} \sin \alpha \left(1 - \frac{z}{z_{\text{lim}}}\right) \quad (59)$$

setting $\Delta z = 0$ for higher altitude than z_{lim}

Since this method is an approximation of the real buoyancy force, we add a corrected factor $\gamma = 6$. We set its value in order to make our model fit with the LMD mesoscale model. Therefore, the buoyancy term f_b of our model becomes :

$$f_b(z) = \gamma \frac{\theta(z) - \theta(z + \Delta z(z))}{\theta(z + \Delta z(z))} g \sin \alpha \quad (60)$$

7.5.4 Friction term

The friction term depends on the slope wind and the eddy coefficient K . This coefficient depends itself on the total wind \vec{v} . A method to calculate this coefficient is given in *Hourdin et al.* (1993) and is the following :

$$K = l e^{\frac{1}{2}} \quad (61)$$

where l is the mixing length, and e is a diagnostic estimation of the turbulent energy such as

$$e = \max \left\{ l^2 \left(\frac{\partial \vec{v}}{\partial z} \right)^2, e_{\text{min}} \right\} \quad (62)$$

where e_{min} is set to $1 \times 10^{-6} \text{m}^2 \cdot \text{s}^{-2}$ and

$$l = \frac{\kappa z}{1 + \frac{\kappa z}{l_{\text{min}}}} \quad (63)$$

with $l_{\text{min}} = 30\text{m}$ and $\kappa = 0.4$ the Von Karman constant.

We assume a logarithmic profile of wind to set K to a given profile, non depending on u or v . In other words we choose :

$$\|\vec{v}\| = \frac{u^*}{\kappa} \ln \left(\frac{z}{z_0} \right) \quad (64)$$

where z_0 is the roughness length and u^* the friction velocity that we set to 1.5 m/s .

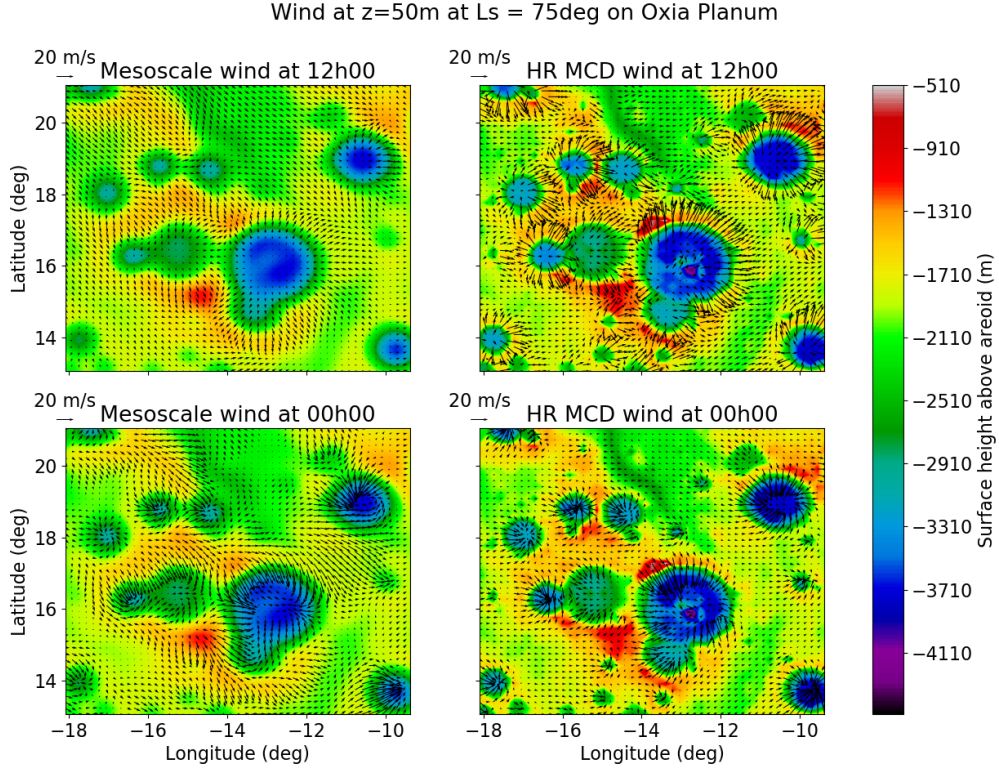


Figure 20: High resolution wind from the MCD (right) compared to the LMD Mesoscale model on left at noon (top) and midnight (bottom) at 50m above surface at Ls=75°

7.5.5 Stationary solution of the equations

Once the system has been discretized, one can put it under matrix form :

$$\begin{cases} \forall l \in [1, N-1], \alpha_l \begin{pmatrix} u_l \\ v_l \end{pmatrix} = \beta_{l+1} \begin{pmatrix} u_{l+1} \\ v_{l+1} \end{pmatrix} + \beta_l \begin{pmatrix} u_{l-1} \\ v_{l-1} \end{pmatrix} + \gamma_l \\ \alpha_N \begin{pmatrix} u_N \\ v_N \end{pmatrix} = \beta_N \begin{pmatrix} u_{N-1} \\ v_{N-1} \end{pmatrix} + \gamma_N \end{cases} \quad (65)$$

with $\alpha_l = \begin{pmatrix} X_{l+1} + X_l & -f\Delta z \\ f\Delta z & X_{l+1} + X_l \end{pmatrix}$, $\beta_l = \begin{pmatrix} X_l & 0 \\ 0 & X_l \end{pmatrix}$ and $\gamma_l = \begin{pmatrix} f_{bl}\Delta z \\ 0 \end{pmatrix}$ such that:

$$\begin{cases} X_{l+1} = \frac{K_{l+\frac{1}{2}}}{z_{l+1} - z_l} \\ \Delta z = z_{l+\frac{1}{2}} - z_{l-\frac{1}{2}} \end{cases}$$

Then we can solve the system of $2N$ equations and find u_l and $v_l \forall l \in [1, N]$ and compare the results with the LMD Mesoscale model. A comparison between the two models is shown on Figure 20.

A Computing Martian Dates and Local Time

In this appendix we briefly describe how one may compute aerocentric solar longitude of Mars for a given Julian date, as well as how to compute corresponding Local True Solar Time.

The equations and methods given here are taken from Capderou (2005) which should be consulted for a detailed description.

A.1 Some constants

| | | |
|-------------|-----------|--|
| N_s | 88775.245 | Number of seconds in a sol (martian day) |
| | 668.6 | Number of sols in a martian year |
| Ls_{peri} | 250.99 | Perihelion date (in deg.) |
| t_{peri} | 485.35 | Perihelion date (in sols) |
| a | 1.52368 | Semi-major axis of orbit (in AU) |
| e | 0.09340 | Orbital eccentricity |
| ϵ | 25.1919 | Obliquity of equator to orbit (in deg.) |

A.2 Computing martian dates and aerocentric solar longitude

A.2.1 The three anomalies

For an elliptical trajectory, the **true anomaly** ν is given by the polar angle of the position, with the convention that $\nu = 0$ at the periastron (minimum distance to center, i.e. the perihelion, in Mars' case).

If $n = 2\pi/T$ is the mean angular frequency of motion (T is the period of revolution, i.e. a year), then at time t (taking the time origin as $t = t_{peri}$, perihelion date at which $\nu = 0$):

$$n(t - t_{peri}) = 2 \arctan \left[\sqrt{\frac{1-e}{1+e}} \tan \frac{\nu(t)}{2} \right] - \frac{e\sqrt{1-e^2} \sin \nu(t)}{1 + e \cos \nu(t)} \quad (66)$$

The **eccentric anomaly** E is related to mean motion n by:

$$n(t - t_{peri}) = E(t) - e \sin E(t) \quad (67)$$

The **mean anomaly** M is the angle determining the position of a fictitious point in uniform circular motion of angular frequency n . Thus,

$$n(t - t_{peri}) = M(t) \quad (68)$$

A.2.2 Aerocentric solar longitude Ls

The position of the planet on its heliocentric orbit is given by the aerocentric solar longitude Ls . The origin of Ls is defined as the vernal equinox (northern hemisphere spring equinox).

Ls is directly related to the true anomaly ν :

$$\nu = Ls - Ls_{peri} \quad (69)$$

where Ls_{peri} is the perihelion date.

A.2.3 Converting Julian date JD to Martian sol number D_s

For a given Julian date JD , the corresponding martian sol date $D_s \in [0; N_s]$ (i.e. number of sols elapsed since beginning of martian year defined by $Ls = 0$):

$$D_s = (JD - JD_{ref}) \frac{86400}{88775.245} \pmod{N_s} \quad (70)$$

where 86400 and 88775.245 are respectively the number of seconds in an earth day and a martian sol. JD_{ref} is a reference Julian date corresponding to an $Ls = 0$ event.
Example of reference date: $Ls = 0$ occurred on 19-12-1975 at 4:00:00, which corresponds to Julian date 2442765.667.

A.2.4 Converting sol number D_s date to Ls

For a given sol number $D_s \in [0; N_s]$, the corresponding value of aerocentric solar longitude Ls may be computed as follows:

Step1: Compute mean anomaly $M(D_s)$ (in radians):

$$M = 2\pi \frac{D_s - t_{peri}}{N_s} \quad (71)$$

Step 2: Compute eccentric anomaly $E(D_s)$ (in radians):

This is the tricky bit (also known as Kepler's problem). Eccentric and mean anomalies are related by the nonlinear equation:

$$M = E - e \sin E \quad (72)$$

which must be solved by, for instance, a Newton iterative procedure.

Step 3: Compute true anomaly $\nu(D_s)$ (in radians) using:

$$\nu = 2 \arctan \left[\sqrt{\frac{1+e}{1-e}} \tan \left(\frac{E}{2} \right) \right] \quad (73)$$

Step 4: Compute $Ls(D_s)$ (in degrees):

$$Ls = \left(\nu \frac{180}{\pi} + Ls_{peri} \right) (mod 360) \quad (74)$$

A.3 Computing Local True Solar Time

The steps required to compute the Local True Solar Time at a given longitude lon (in degrees East) for a given Julian Date are the following:

Step 1: Compute Local Mean Time LMT_0 at longitude 0, in martian hours, for a given Julian date JD :

$$LMT_0 = \left(LMT_{ref} + 24(JD - JD_{ref}) \frac{86400}{88775.245} \right) (mod 24) \quad (75)$$

Where JD_{ref} is a reference Julian date, and LMT_{ref} the Local Mean Time at longitude 0, in martian hours, at that date. 86400 and 88775.245 are respectively the number of seconds in an earth day and a martian sol.

Example of reference date and time: 01-01-1976 at 00:00:00 was such that $JD_{ref} = 2442778.5$ and $LMT_{ref} = 16.1725$.

The equation above assumes simple Keplerian motion and is accurate to a few minutes with respect to more advanced computations which account for the interactions between main objects of the Solar System (see e.g. the "Mars24" website <http://www.giss.nasa.gov/tools/mars24> and documentation).

As of MCDv5.2 and the following version, we use a more elaborate equation to compute LMT_0 for a given JD , as can be seen in the `Mars_LMT0` function in `call_mcd.F` where small corrections are

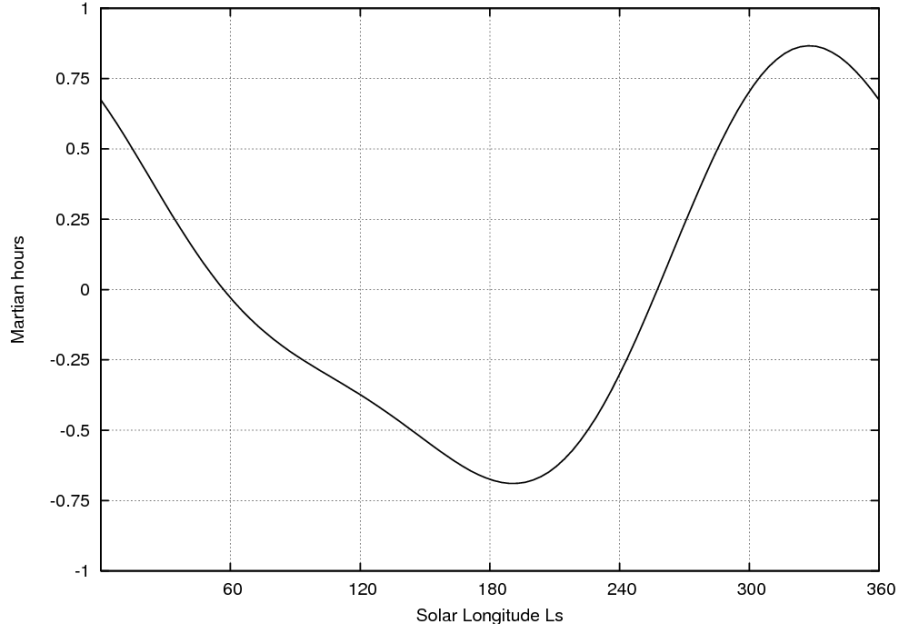


Figure 21: Equation Of Time (EOT) for Mars, showing the difference between Mean Local Time and True Solar Time, as a function of Solar Longitude Ls .

added to obtain a better match with the full computation from "Mars24". We thus obtain a result shown to be accurate to a second or less over the period of Earth years 1950 to 2050.

Step 2: For the given heliocentric solar longitude Ls (which is obtained from Julian Date JD as explained previously), compute the Equation Of Time EOT (which yields, in martian hours, the difference between Mean Time and True Solar Time; see Figure 21) :

$$EOT = \left[2e \sin(Ls - L_{s_{peri}}) - \tan^2\left(\frac{\epsilon}{2}\right) \sin(2Ls) \right] \frac{24}{2\pi} \quad (76)$$

Where $L_{s_{peri}}$ is the perihelion date, e the orbital eccentricity and ϵ the obliquity of equator to orbit.

Step 3: Compute Local True Solar Time at longitude 0, $LTST_0$, in martian hours:

$$LTST_0 = LMT_0 - EOT \quad (77)$$

step 4: At longitude lon (in degrees east), Local True Solar Time $LTST$, in martian hours, is then:

$$LTST = \left(LTST_0 + \frac{lon}{15} \right) (mod\ 24) \quad (78)$$

B Differences Between Version 6.1 and Previous Versions of the MCD

Differences between version 6.1 and version 5.3

- As signaled by the major version number change, the latest updated version of the Mars PCM has been used to generate the database files.
- The vertical resolution of the data base files has been increased to 73 levels (whereas it was 49 levels for MCDv5.x).
- The `call_mcd` routine is now put inside a module `MCD.F90`
- Scenarios MY34 and MY35 are now available
- Implementation of high temporal resolution dust scenarios
- Improvement of dust deposition rate using the high temporal resolution dust opacity
- Calculation of the local slope (inclination and orientation)
- Implementation of the solar irradiance on slopes in high resolution mode
- Implementation of slope winds in high resolution mode
- InSight measurements is now used as reference for high resolution surface pressure (instead of Viking Lander 1 before), including in dust storm cases.
- Correction on the density extrapolation above last model layer.
- Order of extra variables changed.
- Extra variables added : potential temperature, incident solar flux at the top of the atmosphere, reflected solar flux on surface, surface albedo, thermal inertia and perennial water ice.
- Solar fluxes are now rescaled to avoid unrealistic variations due to time interpolation.
- A Python3 interface to the software has been added.
- Scilab and Python2 interfaces to the software were removed.

Differences between version 5.3 and version 5.2

- New EUV min/max/ave scenarios: the bracketing and average Extreme UV forcings from the Sun have been redesigned to be more in line with our knowledge of the recent solar cycles.
- The added small scale perturbation (gravity waves) scheme has been improved to also take into account the horizontal propagation of the gravity wave.
- The evaluation of species column amount, when in high resolution mode, has been improved.
- The extrapolation of density and species volume mixing ratio when above the MCD topmost layer (250km) has been improved.
- The scenario for Mars Year 32 has been added.
- The Matlab interface has been improved and is now fully interactive.
- The values of water ice effective radius (`extvar[45]`) were wrong in MCDv5.2 and have been corrected.

Differences between version 5.2 and version 5.1

- The main changes in MCD version 5.2 are the addition of add-on scenarios for Mars Years 24 to 31, and important fixes concerning vertical velocity, total electronic content and interpolations in the near-surface layer.
- Overall, all the changes that have been introduced are:
 - Added scenarios for Mars Years 24 to 31 (corresponding to values 24 to 31 for `call_mcd` input `scena` parameter).
 - Vertical velocity and associated RMS (`extvar[26]` and `extvar[27]`) have been corrected.
 - Total electronic content (TEC, `extvar[76]`) is better evaluated (using "chemistry ionosphere" electronic content only).
 - The interpolation scheme for the near-surface layer (first few meters above the surface) has been improved.
 - More control when using combined small and large scale perturbation schemes to avoid (rare cases of) unphysically negative density.
 - Added Local Mean Solar Time to outputs (`extvar[11]`)
 - Added Sun-Mars distance to outputs (`extvar[12]`)
 - Added solar zenith angle to outputs (`extvar[56]`)

Differences between version 5.1 and version 5.0

- The main change in MCD version 5.1 is in generation of the underlying dust scenarios to better represent the baseline Martian climatology (scenario "clim", now based on a geometrical mean of several years opacities) and extreme bracketing cases: "cold" (now without radiatively active clouds), "warm", "storm"
- Other changes that have been introduced are:
 - In the MCD software: A near-surface variability scheme has been added to better account for the sub-grid scale effects in the MCD perturbation schemes.
 - In the MCD software: Improved interpolation between the surface and the model lowest layer (5 m) for temperature and winds.
 - In the MCD software: several changes in the output variables array `extvar`, as detailed in the *MCD v5.1 User Manual*.
 - In the GCM: The mean atmospheric composition in Ar and N₂ has been updated to match the latest (2013) Curiosity SAM measurements.
 - In the GCM : Better representation of the water cycle yielding some improvements in the prediction of water vapor, ice and ice particle radii.
 - In the GCM: Improved representation of the extreme UV flux from the Sun.
 - In the GCM: Corrected Boundary layer (nighttime surface layer)
 - In the GCM: Corrected Dynamical scheme (on potential temperature) when CO₂ is condensing or subliming.

Differences between version 5.0 and version 4.3

- The main change in MCD version 5.0 is in the fact that the database files result from simulations using the a completely **new version of the LMD GCM**, which includes many improvements, compared to the version that was used to derive MCDv4.x datafiles. In particular: radiatively active clouds, improved clouds microphysic, semi-interactive dust transport, new dust radiative properties, improved CO₂ cycle, improved convective boundary layer, ionosphere, improved NLTE cooling in the upper atmosphere, etc.

- Other changes which have been introduced are:
 - The EOFs (Empirical Orthogonal Functions) for large scale perturbation scheme are now at higher resolution (32×24 ; twice what was used previously). Moreover, for the “climatology” scenario, EOFs corresponding to the individual (Mars Years 24, 26, 27, 29 and 30) runs are used.
 - Improved interpolation between the surface and the model lowest layer (5 m) for temperature and winds.
 - Many new variables have been included: Columns and volume mixing ratios of Ar, O, O₂, H, H₂, electrons, key parameters concerning the convective planetary boundary layer (PBL), etc.
 - Users may now pick which “extra variables” need be computed and outputted (rather than the all-or-nothing capability of previous MCD software).

Differences between version 4.3 and version 4.2

- The main upgrade in MCD version 4.3 is the improvement of the large scale perturbation model. Version 4.3 thus uses the same database datafiles as version 4.2, except for a subset which contains updated data required for the large scale perturbation model.
- Other changes that have been introduced are:
 - An additional vertical coordinate (‘zkey’ parameter) may be used to specify vertical coordinate as altitude above reference radius (arbitrarily set to 3.39610^6 m).
 - The output unit to which messages are written is now a parameter that can be set by the user (the default output unit is set to 6, which implies, in conformance with Fortran standards, the standard output).
 - In order for the whole MCD to fit in a single DVD, some datafiles (all those which contain data about dust storm scenarios, i.e. files in the `data` directory with names starting with `strm`) have been compressed (gzipped) and should be un-compressed (gunzipped) before being used.

Differences between version 4.2 and version 4.1

- Version 4.2 uses the same database datafiles as version 4.1, except for a small subset (the files which contain variability); most improvements, changes and new features are in the access and postprocessing software.
- The main new features and differences are:
 1. The main Fortran subroutine to retrieve data from the database is now called “call_mcd” and **significant changes to the argument list**, compared to its predecessor “atmemcd”, have been introduced:
 - A new high resolution procedure (based on the integration of high resolution 32 pixels per degree MOLA topography) has been implemented.
 - Input and output arguments which are floating numbers are now declared as **single precision** (i.e. Fortran REAL), except ‘xdate’, which is double precision, (i.e. Fortran REAL*8).
 - The way by which users impose date and local time has changed.
 - Input **longitude and latitude must now be given in degrees**. Longitude is interpreted as degrees east (as before).
 - Input arguments used to signal and generate perturbations have been changed.
 - Day to day variability of atmospheric variables is now given either pressure-wise or altitude-wise, depending on the vertical coordinate selected by the user.

2. Examples of interface software for C, C++ and Scilab users, have been added (in addition to the pre-existing IDL and Matlab ones).
3. Computation of solar longitude (from a given Julian date) has been made more accurate. Computation of local time (given in true solar time) has been improved by using an appropriate equation of time.
4. The “pres0” tool has been updated.

Lists of changes and improvements of previous versions of the MCD

- Version 4.1 is similar to beta version 4.0 with some improvements and a few problems fixed.
- The main differences between version 4 and previous version 3.1 are:
 1. The database now extends up to the thermosphere and new variables (upper atmospheric composition: CO₂, N₂, CO, O, H₂ and, in the lower atmosphere: water, water ice, ozone, dust) are available.
 2. Different vertical coordinates may be specified as input, including pressure level.
 3. A linear interpolation in time (*Ls*) for mean variables between seasons was added.
 4. For some variables, an estimation of the “day to day” variation is provided (root mean square values).
 5. There is a significant re-arrangement of arguments of atmemcd so that all the input variables are followed by all the output variables.
 6. We suggest the use of direct compilation rather than using the UNIX command “make”.
 7. Variables are now saved in atmemcd to fix problems with F77 compilers which don’t store values of variables between subroutine calls.
 8. The database now has a more accurate representation of gravity; the fact that it varies following an inverse square law is accounted for when integrating the hydrostatic equation. The variation of *R*, the gas constant, with altitude is also taken into account.
 9. The horizontal resolution of the database has changed to $5.625^\circ \times 3.75^\circ$ (longitude \times latitude).
 10. We now provide the separate tool to compute surface pressure with high accuracy.
 11. We now provide some tool to use the database software from IDL.
- A major change in Version 3.1, compared to version 3.0 of the database, is the change from DRS data format to NetCDF. A bug was also fixed for the calculation of large scale variability in the upper atmosphere (above 120 km).
- The main differences between version 3.0 and 2.3 are mostly related to the content of the database files, due in particular to improvements made in the models used to build the database, including an extension of the model top from 80 to 120 km, improved surface properties and a dust scenarios from Mars Global Surveyor.
- The main difference between version 2.3 and 2.0 is the use of the main subroutine ATMEMCD which computes meteorological variables from the Mars Climate Database (MCD).
- The main difference between version 2.0 and 1.0 of the MCD is that the large-scale variability model now makes use of two-dimensional, multivariate Empirical Orthogonal Functions (EOFs). These now describe correlations in the model variability as a function of both height and longitude (rather than solely of height as in version 1.0).